Afadin Signaling at the Spinal Neuroepithelium Regulates Central Canal Formation and Gait Selection

Sophie Skarlatou, Coralie Hérent, Elisa Toscano, César Mendes, Julien Bouvier, Niccolò Zampieri

Cell Reports

Article

Afadin Signaling at the Spinal Neuroepithelium Regulates Central Canal Formation and Gait Selection

Graphical Abstract

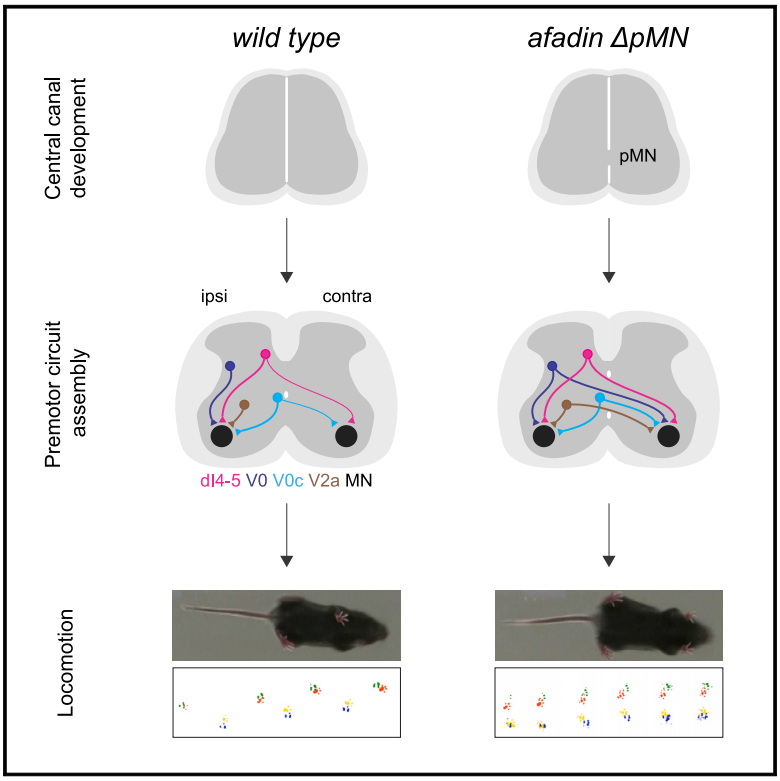

Authors

Sophie Skarlatou, Coralie Hérent, Elisa Toscano, César S. Mendes, Julien Bouvier, Niccolò Zampieri

Correspondence

niccolo.zampieri@mdc-berlin.de

In Brief

Skarlatou et al. report that afadin function in the developing spinal neuroepithelium controls organization of the midline. Afadin elimination from the motor neuron progenitor zone results in duplication of the central canal, aberrant wiring of dI4-5, V0, and V2a premotor neurons, and loss of left-right limb alternation.

Highlights

- Afadin elimination from motor neuron progenitors causes hopping phenotype
- Afadin function at the neuroepithelium controls organization of spinal midline
- Miswiring of dI4-5, V0, and V2a premotor interneurons in afadin mutant mice

Skarlatou et al., 2020, Cell Reports *31*, 107741
June 9, 2020
https://doi.org/10.1016/j.celrep.2020.107741

CellPress

Cell Reports

CellPress
OPEN ACCESS

Article

Afadin Signaling at the Spinal Neuroepithelium Regulates Central Canal Formation and Gait Selection

Sophie Skarlatou,[1,2] Coralie Hérent,[3] Elisa Toscano,[2] César S. Mendes,[4] Julien Bouvier,[3] and Niccolò Zampieri[1,2,5,*]
[1]Cluster of Excellence NeuroCure, Charité-Universitätsmedizin Berlin, Charitéplatz 1, 10117 Berlin, Germany
[2]Max Delbrück Center for Molecular Medicine, Robert-Rössle-Str. 10, 13125 Berlin, Germany
[3]Paris-Saclay Institute of Neuroscience, UMR 9197 CNRS & Université Paris-Saclay, Avenue de La Terrasse, 91190 Gif sur Yvette, France
[4]CEDOC, Faculdade de Ciências Médicas, Universidade Nova de Lisboa, 1169-056 Lisboa, Portugal
[5]Lead Contact
*Correspondence: niccolo.zampieri@mdc-berlin.de
https://doi.org/10.1016/j.celrep.2020.107741

SUMMARY

Afadin, a scaffold protein controlling the activity of the nectin family of cell adhesion molecules, regulates important morphogenetic processes during development. In the central nervous system, afadin has critical roles in neuronal migration, axonal elongation, and synapse formation. Here we examine the role of afadin in development of spinal motor circuits. Afadin elimination in motor neuron progenitors results in striking locomotor behavior: left-right limb alternation is substituted by synchronous activation, characteristic of bound gait. We find that afadin function at the neuroepithelium is required for structural organization of the spinal midline and central canal morphogenesis. Perturbation of afadin results in formation of two central canals, aberrant contralateral wiring of different classes of spinal premotor interneurons, and loss of left-right limb alternation, highlighting important developmental principles controlling the assembly of spinal motor circuits.

INTRODUCTION

The ability to generate coordinated and adaptable movements is essential for survival. In vertebrates, spinal motor circuits orchestrate execution of complex motor programs by integrating descending commands and sensory information to activate biomechanically coherent ensembles of motor neurons in precise sequences (Kiehn, 2006; Goulding, 2009; Arber, 2012). Several classes of interneurons in the spinal cord are involved in wiring of circuits at the basis of motor function, such as coordination of antagonist muscle contraction and left-right alternation of limb movements (Grillner and Jessell, 2009; Gosgnach et al., 2017). Spinal networks controlling the rhythm and pattern of muscle contraction provide a substrate for different locomotor actions ranging from swimming to walking and running. In this context, the relative timing of limb activation is a key element for the control of gait selection in tetrapods (Grillner, 2006; Kiehn, 2016). However, despite the importance of spinal circuits regulating the coordination of limb movement, the principles controlling their assembly and function are not completely understood.

Mouse genetic analysis has revealed specific functions for different spinal interneuron classes in gait control. V0 neurons originating from Dbx1 progenitors have important roles in the coordination of left-right limb movements (Lanuza et al., 2004). Inhibitory $V0_D$ neurons have been linked to generation of alternating patterns at low frequencies of locomotion, whereas excitatory $V0_V$ neurons control alternation at higher locomotor frequencies (Talpalar et al., 2013). V2a neurons have been shown to influence gait selection depending on the speed of locomotion (Crone et al., 2008, 2009). In addition, roles in coordinating limb activity have been proposed for V3 neurons (Zhang et al., 2008). However, teasing out the precise composition and wiring of spinal motor circuits has been challenging because of the limited ability to selectively access and interrogate the function of discrete neuronal subtypes and circuits *in vivo*.

Several studies have highlighted the importance of axon guidance molecules such as netrins, slits, and ephrins in directing neuronal connectivity across the neuraxis as a developmental strategy to regulate wiring of spinal circuits (Chédotal, 2019). In particular, ephrin B3 expression at the midline of the hindbrain and spinal cord has been shown to provide a repulsive signal that controls unilateral wiring of EphA4-expressing axons (Kullander et al., 2001). As a consequence, genetic manipulation of ephrin B3-EphA4 signaling results in a dramatic switch from alternation to synchronous activation of limbs (Kullander et al., 2003; Beg et al., 2007; Iwasato et al., 2007). These studies elucidate some of the molecular underpinnings controlling the development of circuits for left-right alternation but also offer an entry point for identification of neurons contributing to these networks. Indeed, selective ablation of EphA4 in spinal excitatory interneurons has been shown to be sufficient to perturb left-right alternation (Borgius et al., 2014). Moreover, elimination of EphA4 expression in spinal interneurons derived from the Lbx1 progenitor domain results in their aberrant bilateral wiring and in a

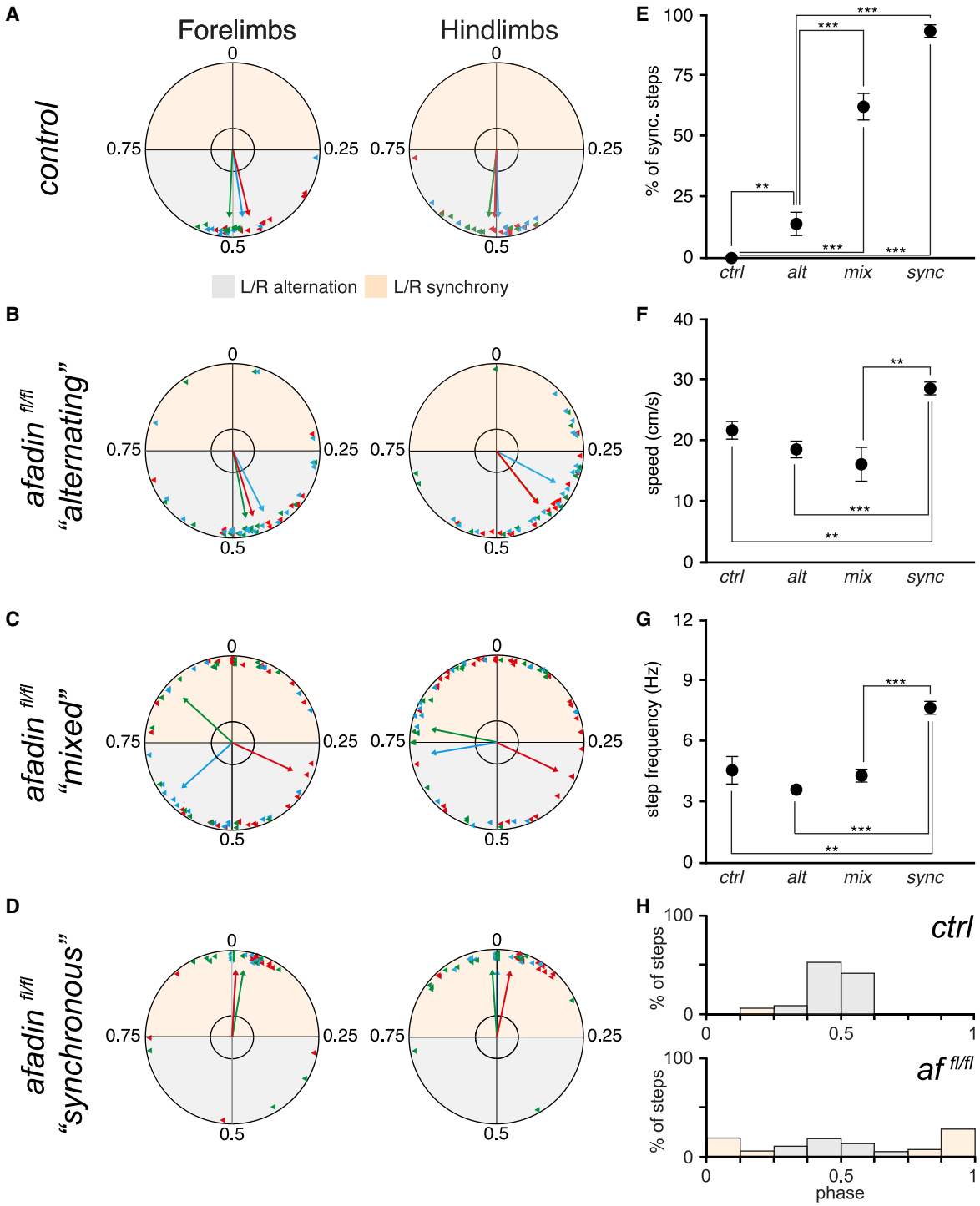

Figure 1. Loss of Left-RightLimb Alternation in Afadin Mutant Mice

(A) Circular plots showing the phase relationship of fore- and hindlimb movements and the average orientation vector of three individual control mice. The gray area indicates alternation and the orange area synchrony.

(B) Circular plots showing the phase relationship of fore- and hindlimb movements and the average orientation vector of three individual *afadin* $^{fl/fl}$ mice with the "alternating" phenotype.

(C) Circular plots showing the phase relationship of fore- and hindlimb movements and the average orientation vector of three individual *afadin* $^{fl/fl}$ mice with the "mixed" alternating and synchronous phenotype.

(legend continued on next page)

context-dependent switch to left-right synchrony (Satoh et al., 2016).

In this study, we set out to investigate the consequences of afadin elimination for the development of spinal motor circuits. Afadin, a scaffold molecule coordinating adhesive function of the nectin and classical cadherin families, has been shown to be involved in the control of neuronal migration and positioning, axonal guidance, and synapse formation (Okabe et al., 2004; Beaudoin et al., 2012; Gil-Sanz et al., 2014; Dewitz et al., 2018). We eliminated afadin from motor neuron progenitors and found that alternation of limb movement is substituted by synchronous activation. To understand the mechanism underlying this phenotype, we studied spinal cord development and assembly of motor circuits in afadin mutant mice. Our data indicate that afadin expression at the neuroepithelium is necessary for lumen formation during development and that its elimination from the motor neuron progenitor zone results in generation of two central canals. As a consequence, the structural integrity of the spinal cord midline is compromised, and the wiring of motor circuits is altered. We identified aberrant contralateral connectivity patterns of dI4-5, V0, V0c, and V2a spinal premotor interneurons, underlining their importance for the control of gait selection.

RESULTS

Loss of Left-Right Limb Alternation in Afadin Mutant Mice

In previous work, we eliminated afadin from mouse motor neurons by crossing a copy of a floxed allele and a copy of a null allele with the *olig2::cre* driver line to achieve selective deletion from motor neurons. However, *afadin* $^{fl/-}$ *; olig2::cre*$^{+/-}$ (*afadin* $^{fl/-}$) mice die at perinatal stages because of severe hydrocephalus, precluding analysis of motor behavior (Dewitz et al., 2018). To extend the lifespan, we generated a fully conditional afadin model (*afadin* $^{fl/fl}$; *olig2::cre*$^{+/-}$ mice, hereafter referred to as *afadin* $^{fl/fl}$; Figures S1A and S1B). *Afadin* $^{fl/fl}$ mice are born at expected Mendelian frequency and display a defect in the pattern of activation of left-right limbs during on-ground locomotion.

We performed quantitative gait analysis to precisely characterize the locomotor phenotype of afadin mutant mice (Mendes et al., 2015). Control animals exclusively used alternation of left-right limbs during locomotion, a characteristic feature of a normal walking gait (Figures 1A and 1E; Video S1). In contrast, we observed that one-third of mutant mice mostly used alternating steps but showed a significant increase in the incidence of synchronous ones (Figures 1B and 1E; Video S2), another third presented bouts of alternating and synchronous steps (Figures 1C and 1E; Video S3), and the remaining animals showed constant synchronous activation of left and right limbs (Figures 1D and 1E; Video S4). In this last cohort, step frequency and locomotor speed were significantly increased to values characteristic of boundgait (Figures 1F and 1G; Bellardita and Kiehn, 2015; Lemieux et al., 2016). These data indicate that afadin elimination perturbs the circuits controlling coordination of left-right limb movement, resulting in loss of alternation in favor of synchronous activation (Figure 1H).

Afadin Mutant Mice Show Abnormal Left-Right Alternation in Isolated Spinal Cord Preparations

Next we asked whether the phenotype observed in afadin mutant mice depends exclusively on spinal motor circuits and analyzed fictive locomotor activity in isolated lumbar spinal cord preparations from newborn mice (Figure 2A; Kjaerulff and Kiehn, 1996). In control experiments, induction of locomotor-like activity following application of N-methyl-D-aspartate and serotonin produced clear alternating patterns in left (l) and right (r) lumbar (L) roots (Figures 2B and 2C). In agreement with the behavioral data, preparations from *afadin*$^{fl/fl}$ mice presented a defect in generation of the left-right alternating pattern, ranging from complete synchrony to less penetrant phenotypes characterized by bouts of alternation intermixed with bouts of synchrony (Figures 2D and 2E). In contrast, the pattern of rL2-rL5 roots, which is used as a correlate for flexor-extensor muscle activities, was not affected in mutant spinal cords (Figures 2B and 2D).These experiments suggest that loss of left-right alternation in afadin mutant mice is due to changes in spinal motor circuits and does not require sensory or supraspinal input.

Afadin Elimination Does Not Affect Motor Neuron Development

We next considered how afadin elimination influences gait selection. The precision of motor neuron spatial organization in the spinal cord is thought to be an important determinant for assembly of motor circuits (Sürmeli et al., 2011; Bikoff et al., 2016). We previously observed defects in motor neuron positioning in *afadin* $^{fl/-}$ embryos; thus, we investigated motor neuron generation, identity, and positional organization in fully conditional afadin mice (Dewitz et al., 2018).

We did not find any disruption in the generation and specification of motor neurons in *afadin* $^{fl/fl}$ embryos (Figures S1C). Three-dimensional positional analysis was used to assess motor neuron spatial organization, and we observed perturbation in the divisional segregation of the lateral motor column (LMC) in *afadin* $^{fl/fl}$ embryos (Figures S1D–S1I; Dewitz et al., 2018). Medio-lateral distribution and average settling position analyses showed selective impairment of lateral (LMCl) motor neurons migration, as found previously in *afadin* $^{fl/-}$ mice, but with a significantly lower phenotypic penetrance (Figures S1J and S1K).

(D) Circular plots showing the phase relationship of fore- and hindlimb movements and the average orientation vector of three individual *afadin* $^{fl/fl}$ mice with the "synchronous" phenotype.

(E) Average percentage of synchronous steps in control, *afadin* $^{fl/fl}$ (alt), *afadin* $^{fl/fl}$ (mix), and *afadin* $^{fl/fl}$ (sync) mice (mean ± SEM; t test, $^{**}p < 0.01$, $^{***}p < 0.001$; n = 3 for each genotype).

(F) Average speed in control, *afadin* $^{fl/fl}$ (alt), *afadin* $^{fl/fl}$ (mix), and *afadin* $^{fl/fl}$ (sync) mice (mean ± SEM; t test, $^{**}p < 0.01$, $^{***}p < 0.001$; n = 3 for each genotype).

(G) Average step frequency in control, *afadin* $^{fl/fl}$ (alt), *afadin* $^{fl/fl}$ (mix), and *afadin* $^{fl/fl}$ (sync) mice (mean ± SEM; t test, $^{**}p < 0.01$, $^{***}p < 0.001$; n = 3 for each genotype).

(H) Phase distribution histogram for all the steps analyzed in control mice (top panel, n = 3) and *afadin* $^{fl/fl}$ mice (bottom panel, n = 9).

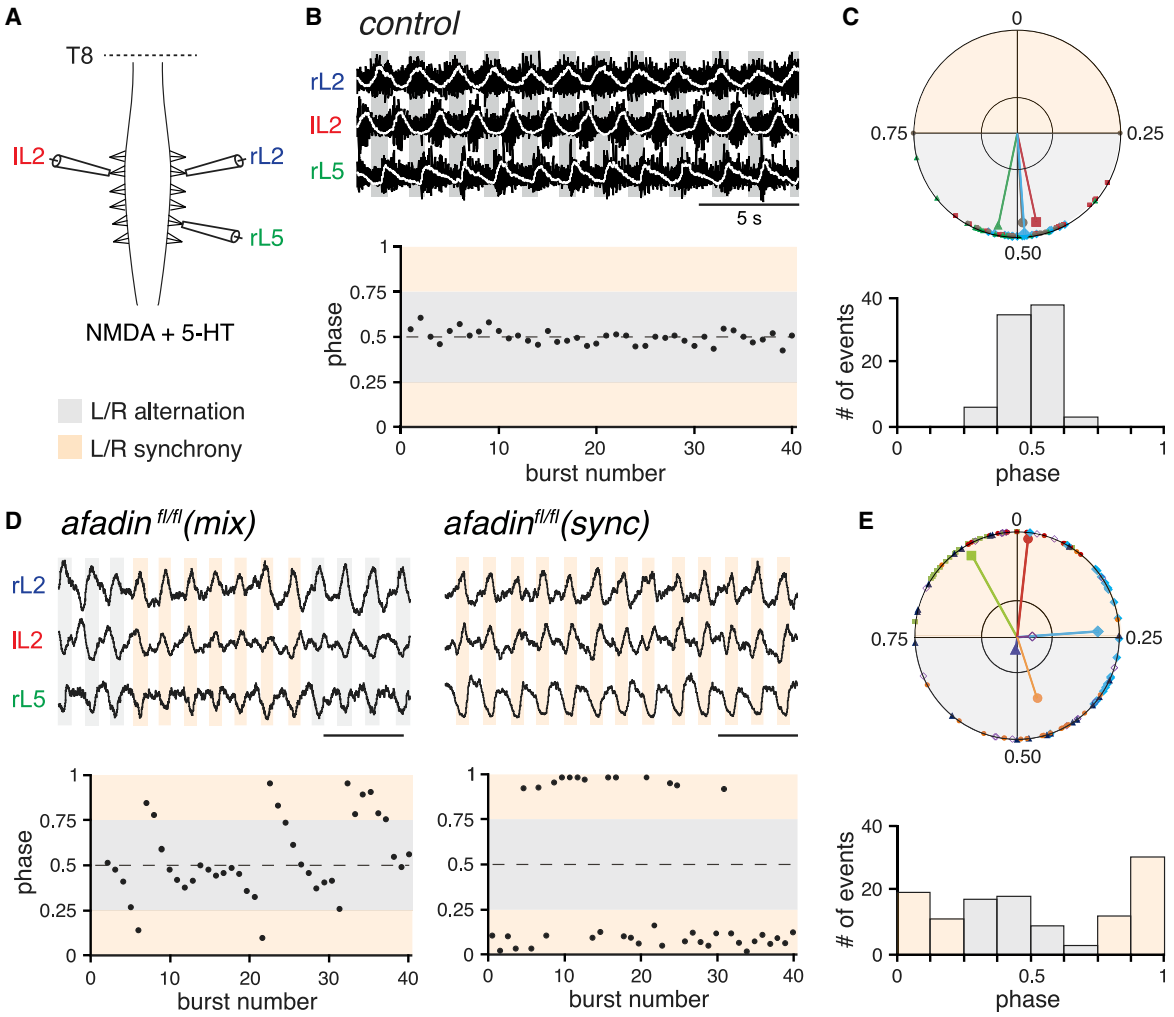

Figure 2. Afadin Mutant Mice Show Abnormal Left-Right Alternation in Isolated Spinal Cord Preparations

(A) *Exvivo* lumbar spinal cord preparation from neonatal mice (0–3 days) spanning lower thoracic to sacral segments. Simultaneous recordings were performed from the left and right second lumbar ventral roots (rL2 and lL2, flexor-related) and the right fifth lumbar ventral root (rL5, extensor-related) using extracellular glass pipettes.

(B) Top panel: recordings of the rL2, lL2, and rL5 roots from a control animal during locomotor-like activity. Raw (black) and integrated (white) activities are superimposed. Grey bars show alternation between rL2/lL2 and rL2/rL5 roots. Bottom panel: locomotor phase between rL2 and lL2 over 40 consecutive bursts from the same animal as above. The gray area indicates alternation and the orange area synchrony.

(C) Top panel: circular plot showing the rL2/lL2 phase-relationship for 80 locomotor cycles and average orientation vectors of four individual control animals. Bottom panel: phase distribution histogram between rL2 and lL2 for all events shown in the circular plot.

(D) Top panel: integrated activities of the rL2, lL2, and rL5 L roots from two *afadin* $^{fl/fl}$ cords during locomotor-like activity. Bottom panel: locomotor phase between rL2 and lL2 over 40 consecutive bursts from the same animals as above. Example 1 (left) shows episodes of alternation and synchrony, whereas example 2 (right) shows only synchronized bursts.

(E) Top panel: circular plot showing the rL2/lL2 phase relationship for 120 locomotor cycles and average orientation vectors of six individual *afadin* $^{fl/fl}$ animals. Bottom panel: phase distribution histogram between rL2 and lL2 for all events shown in the circular plot.

Next we studied motor neuron organization in adult mice. Because transcription factors defining motor neuron subtype identities are no longer expressed at postnatal stages, we assessed the position of medial and lateral LMC neurons using retrograde labeling of cell bodies by muscle injection of the cholera toxin B subunit (CTB). We chose the gastrocnemius (GS) and tibialis anterior (TA) muscles to label a medial and a lateral motor pool. We found CTB-labeled TA and GS motor neurons at the expected rostral lumbar levels of the spinal cord (Figures S1L and S1M; McHanwell and Biscoe 1981; Sürmeli et al., 2011). Transverse and coronal contour analyses showed that the two pools were clustered and clearly segregated from each other (Figures S1N–S1Q). Accordingly, no significant difference was observed in average settling positions and correlation analysis indicated conservation of motor neuron spatial organization in control and *afadin* $^{fl/fl}$ mutant mice (Figures S1R–S1T).

Altogether, these data indicate that elimination of afadin from motor neurons causes a developmental delay in their positioning

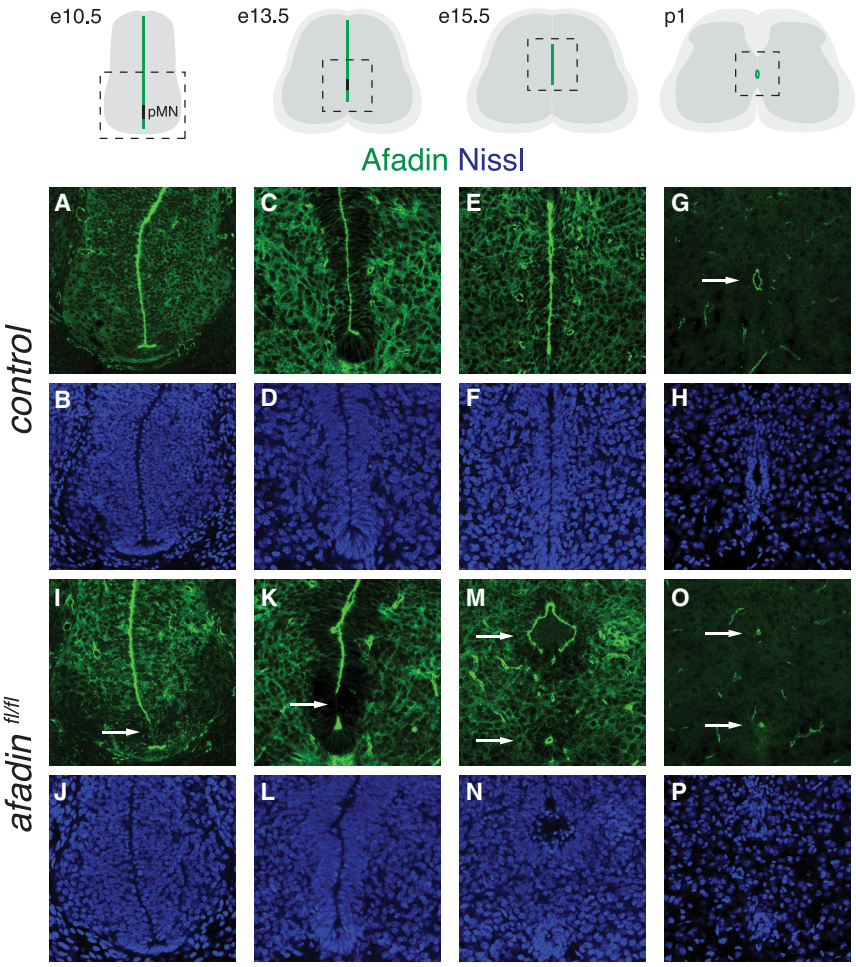

Figure 3. Afadin Mutant Mice Present a Double Central Canal Phenotype

(A–H) Afadin expression in E10.5 (A and B), E13.5 (C and D), E15.5 (E and F), and P1 (G and H) control spinal cords. The arrow in (G) points to the central canal.

(I–P) Afadin expression in E10.5 (I and J), E13.5 (K and L), E15.5 (M and N), and P1 (O and P) *afadin* $^{fl/fl}$ spinal cords. Arrows in (I) and (K) point to the pMN. Arrows in (M) and (O) point to the central canals.

that is resolved during late embryonic development and no longer apparent at postnatal stages.

Afadin Mutant Mice Present a Double Central Canal Phenotype

The absence of a motor neuron positioning defect in adult *afadin* $^{fl/fl}$ mice suggests that the locomotor phenotype does not depend on changes in motor pool organization, raising the question of how afadin elimination affects gait selection. Afadin is ubiquitously expressed in the spinal cord during embryonic development, with higher levels found at the neuroepithelium (Figures 3A–3F and S2A–S2D). Conditional elimination of afadin using the *olig2::cre* allele results in its loss in motor neuron progenitors, suggesting that lack of afadin function at the neuroepithelium might be responsible for the locomotor phenotype (Figures 3I–3L, S2G, and S2H). To test this hypothesis, we analyzed afadin expression during spinal cord development. We observed that, until embryonic day 13.5 (E13.5), the neuroepithelium extends along the whole dorsoventral axis of the spinal cord (Figures 3A–3D, S2A, and S2B). At E14.5 it starts constricting, and the tubular structure of the central canal is clearly visible by postnatal day 1 (P1) (Figures 3E–3H, S2C–S2F, and S2M–S2O). Afadin is localized at the neuroepithelium lining the midline during embryonic development and remains expressed around the central canal until adult stages. In mutant embryos, afadin expression is eliminated from the motor neuron progenitor zone (pMN) as early as E10.5 while remaining unaffected in the rest of the neuroepithelium (Figures 3I–3L, S2G, and S2H). At E14.5, we observed a clear disruption in the morphology of the midline, resulting in formation of two independent tubular structures above and below the pMN (Figures 3M, 3N, S2I, S2J, and S2P). As a result, a double central canal is evident by P1 and maintained into adult stages (Figures 3O, 3P, S2K, S2L, S2Q, and S2R; data not shown). These data suggest that afadin function at the neuroepithelium is required for central canal formation.

Afadin Regulates Development of the Spinal Cord Midline

To examine whether afadin has a general role in the organization of midline structures during development, we generated a conditional mutant using the *Wnt1::cre* line, which recombines in dorsal spinal cord progenitors (*af* $^{fl/fl}$ *Wnt1*; Rowitch et al., 1999). *Af* $^{fl/fl}$ *Wnt1* mice die at late embryonic stages as a result of exencephaly. At E14.5, we observed a reduction in the dorso-ventral extent of afadin and phalloidin expression at the neuroepithelium of mutant mice (Figures 4E and S3A–S3D). The defect was significantly more pronounced at E16.5 (Figures 4A–4E). In addition, we found that the extent of the dorsal gray matter at the midline was significantly increased whereas the ventral one was reduced, resulting in a ventral shift in positioning of the developing central canal in *af* $^{fl/fl}$ *Wnt1* mice (Figures 4A, 4B, 4F–4K, S3E, and S3F). Thus, elimination of afadin from dorsal progenitors also affects anatomical organization of the midline.

Next, to directly test whether afadin function in motor neuron progenitors is required for the double central canal and locomotor phenotypes, we eliminated afadin using the *ChAT::cre* allele, which selectively recombines in postmitotic motor neurons, sparing the progenitor zone (*af* $^{fl/fl}$ *ChAT*; Rossi et al., 2011). *Af* $^{fl/fl}$ *ChAT* mice are born at expected Mendelian frequency, do not show any defect in central canal development, and present a normal alternating locomotor pattern (Figures 4L–4P). These data indicate that afadin plays an important role in

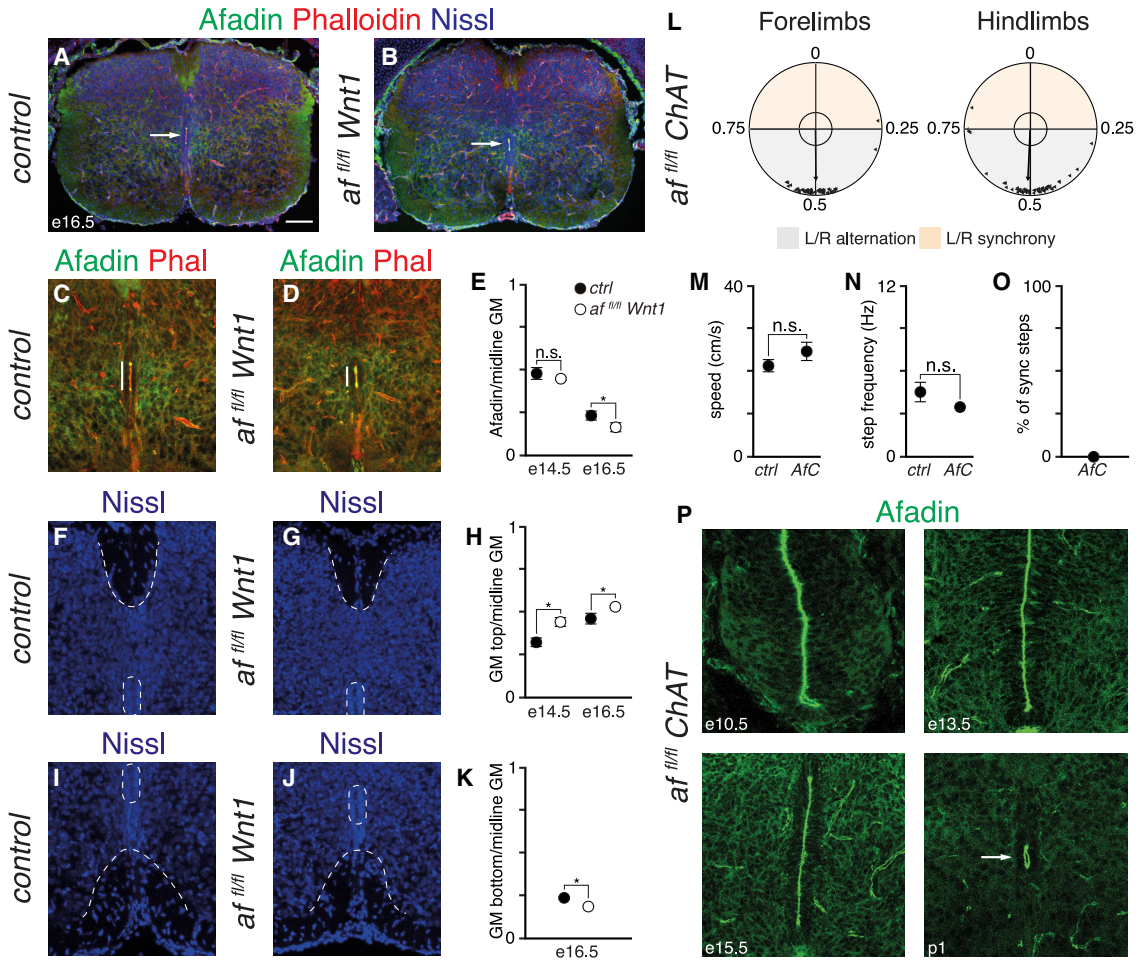

Figure 4. Afadin Function at the Neuroepithelium Regulates Development of the Spinal Cord Midline

(A and B) Transverse sections of an E16.5 control (A) and *afadin* $^{fl/fl}$ *Wnt1* (B) spinal cords. Arrows point to the central canal. Scale bar, 100 μm.

(C and D) Afadin and phalloidin expression in the central canal area of E16.5 control (C) and *afadin* $^{fl/fl}$ *Wnt1* (D) spinal cords. Bars represent the extent of afadin/phalloidin expression.

(E) Quantification of afadin expression at the midline in E14.5 and E16.5 control and *afadin* $^{fl/fl}$ *Wnt1* spinal cords (mean ± SEM; t test, *$p < 0.05$; n = 3).

(F and G) High magnification of the dorsal midline area in E16.5 control (F) and *afadin* $^{fl/fl}$ *Wnt1* (G) spinal cords. Dashed lines delineate the neuroepithelium and the border between the dorsal gray and white matter.

(H) Quantification of the extent of dorsal gray matter in E14.5 and E16.5 control and *afadin* $^{fl/fl}$ *Wnt1* spinal cords (mean ± SEM; t test, *$p < 0.05$; n = 3).

(I and J) High magnification of the ventral midline area in E16.5 control (I) and *afadin* $^{fl/fl}$ *Wnt1* (J) spinal cords. Dashed lines delineate the neuroepithelium and the border between the ventral gray and white matter.

(K) Quantification of the extent of ventral gray matter in e16.5 control and *afadin* $^{fl/fl}$ *Wnt1* spinal cords (mean ± SEM; t test, *$p < 0.05$; n = 3).

(L) Circular plots showing the phase relationship of fore- and hindlimb movements and the average orientation vector in *af* $^{fl/fl}$ *ChAT* mice (n = 3).

(M) Average speed in control and *af* $^{fl/fl}$ *ChAT* mice (mean ± SEM; t test, $p > 0.05$; n = 3).

(N) Average step frequency in control and *af* $^{fl/fl}$ *ChAT* mice (mean ± SEM; t test, $p > 0.05$; n = 3).

(O) Average percentage of synchronous steps in *af* $^{fl/fl}$ *ChAT* mice (mean ± SEM; n = 3).

(P) Afadin expression in E10.5, E13.5, E15.5, and p1 *af* $^{fl/fl}$ *ChAT* spinal cords. The arrow points to the central canal.

maintaining neuroepithelial organization along the spinal midline and that its elimination from the pMN results in double central canal formation and perturbation of circuits controlling left-right alternation.

Midline Expression of Netrin 1 and Ephrin B3 Is Perturbed in Afadin Mutants

The locomotor and anatomical phenotypes observed in *afadin* $^{fl/fl}$ mice raise the question of whether the signals controlling axonal guidance across the midline are perturbed. Netrin 1 and ephrin B3 are prominent examples of such molecules (Serafini et al., 1996; Kullander et al., 2001). Disruption of netrin 1 or ephrin B3 signaling results in loss of left-right limb alternation (Kullander et al., 2003; Rabe et al., 2009). Thus, we examined the expression of these molecules in *afadin* $^{fl/fl}$ mutant mice.

In control mice, netrin 1 is localized in the ventral part of the midline ranging from the central canal to the white matter

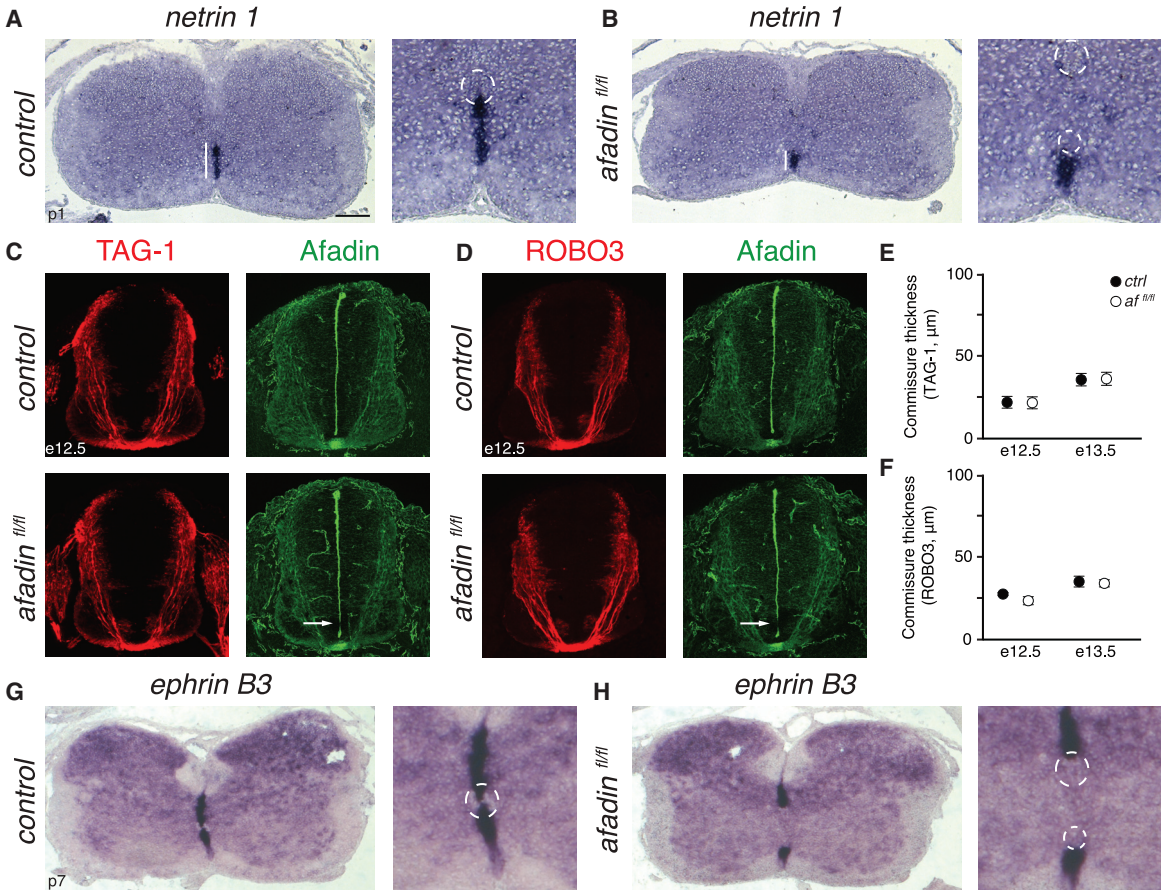

Figure 5. Midline Expression of Netrin 1 and Ephrin B3 Is Perturbed in Afadin Mutants

(A and B) Left panel: netrin 1 mRNA expression in P1 control (A) and *afadin* $^{fl/fl}$ (B) spinal cords. Right panel: magnification of the ventral midline area below the central canal. The central canal is delineated by a dashed line. The bar represents the extent of netrin 1 expression. Scale bar, 100 µm.

(C) Transverse sections of an E12.5 control and *afadin* $^{fl/fl}$ spinal cords showing TAG-1 (left) and afadin (right) expression. The arrow points to the pMN.

(D) Transverse sections of an E12.5 control and *afadin* $^{fl/fl}$ spinal cords showing ROBO3 (left) and afadin (right) expression. The arrow points to the pMN.

(E) Quantification of TAG-1^{+} ventral commissure thickness in E12.5 and E13.5 control and *afadin* $^{fl/fl}$ spinal cords (mean ± SEM; t test, $p > 0.05$; $n = 2$).

(F) Quantification of ROBO3^{+} ventral commissure thickness in E12.5 and E13.5 control and *afadin* $^{fl/fl}$ spinal cords (mean ± SEM; t test, $p > 0.05$; $n = 2$).

(G and H) Left panel: ephrin B3 mRNA expression in a P7 control (G) and *afadin* $^{fl/fl}$ (H) spinal cord. Right panel: magnification of the central canal area. The central canal is delineated by a dashed line.

(Figure 5A). The presence of a double central canal in afadin mutant mice resulted in a reduction in the extent of netrin 1 expression, raising the possibility that development of commissural axons could also be perturbed (Figure 5B). To address this question, we analyzed TAG-1 and ROBO3 expression and localization in the spinal cord of afadin mutant mice, and we did not observe any difference in the trajectory of commissural axons approaching the floor plate or in the thickness of the ventral commissure (Figures 5C–5F and S4A–S4D).

Next, we examined ephrin B3 expression. In control mice, ephrin B3 was localized along the whole dorsoventral extent of the spinal cord gray matter above and below the central canal (Figures 5G). In contrast, in *afadin* $^{fl/fl}$ mice, ephrin B3 expression was absent between the two central canals (Figures 5H). Moreover, this phenotype is tightly linked to the central canal defect because localization of ephrin B3 at the midline of *af* $^{fl/fl}$ *ChAT* mice was not affected (Figure S4E).

Aberrant Wiring of Premotor Circuits in Afadin Mutant Mice

Ephrin B3 serves as a molecular barrier that prevents EphA4-expressing neurons from sending axons to the contralateral side of the spinal cord (Kullander et al., 2001). The disruption in expression of ephrin B3 raises the possibility that the defect in left-right limb coordination could result from aberrant midline crossing of ipsilaterally projecting neurons expressing EphA4 (Paixão et al., 2013; Borgius et al., 2014). Indeed, we observed an increase in contralaterally projecting axons in *afadin* $^{fl/fl}$ mice as early as E15.5 (Figures S4F and S4G). Dorsal premotor interneurons originating from the Lbx1 progenitor domain have been shown to aberrantly connect to contralateral motor neurons upon disruption of ephrin B3-EphA4 signaling (Satoh et al., 2016). Thus, we analyzed premotor connectivity using rabies virus (RV) monosynaptic tracing (Wickersham et al., 2007). Expression of RV glycoprotein (G) in motor neurons was obtained using the

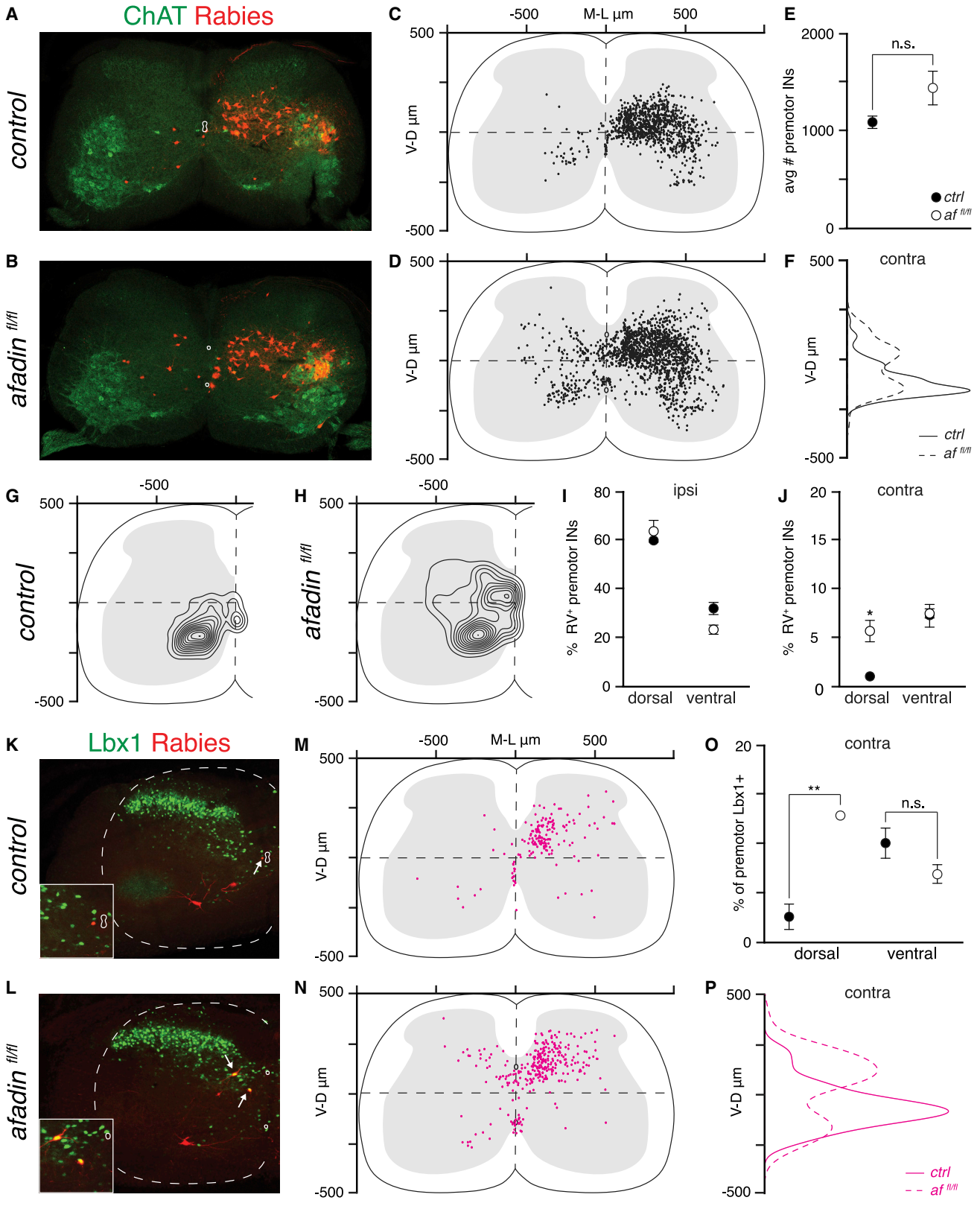

(legend on next page)

Rosa-lsl-G-ires-TVA line (*RΦGT*; Takatoh et al., 2013) and monosynaptic tracing by muscle injection of G-deficient RV (RVΔG-mCherry). Efficient labeling of neurons was observed in control and *afadin* $^{fl/fl}$ mice (Figures 6A, 6B, and 6E; Table S1). To quantitatively analyze the spatial organization of premotor interneurons, we digitally reconstructed their three-dimensional positions and compared their distributions. In control mice, most premotor interneurons were located ipsilaterally in Rexed laminae VI, VII, and X, whereas on the contralateral side, they were mainly confined to lamina VIII, as described previously (Figures 6C, 6G, and S5A; Stepien et al., 2010). The overall distribution of premotor interneurons in *afadin* $^{fl/fl}$ mice was similar; however, an increase in the incidence of contralateral neurons was clearly evident (Figures 6D, 6H, and S5B). We found a significantly higher number of premotor interneurons in the dorsal contralateral quadrant, but we did not observe differences in the numbers of labeled cells in other quadrants (Figures 6F, 6I, 6J, S5C, and S5D).

We next analyzed the connectivity of Lbx1-expressing premotor interneurons and found an ectopic cluster in the dorsal contralateral side of *afadin* $^{fl/fl}$ mice (Figures 6K–6N, S5E, and S5F). Quantitative analysis confirmed this observation and revealed that significantly more Lbx1^{+} premotor neurons are present in the dorsal contralateral quadrant in mutant mice, whereas no significant difference was found in the number of cells labeled in the ventral one (Figure 6O). Accordingly, distribution analysis of contralateral Lbx1^{+} premotor neurons revealed a dorsal peak in *afadin* $^{fl/fl}$ mice (Figure 6P). Altogether, these data reveal the presence of an ectopic cluster of contralateral interneurons in mutant mice, some of which originate from the Lbx1 progenitor zone, as predicted by perturbation of ephrin B3 signaling at the midline.

Multiple Cardinal Interneuron Subtypes Are Miswired in Afadin Mutant Mice

Comparison of total and Lbx1^{+} premotor interneuron maps in *afadin* $^{fl/fl}$ mice indicated the presence of other populations of ectopically wired interneurons (Figures S6A and S6B). Thus, we expanded our analysis to other subtypes implicated previously in the control of locomotion for which markers are available at early postnatal stages (Lu et al., 2015; Ziskind-Conhaim and Hochman, 2017).

First, we focused on interneurons arising from the V0 progenitor domain. In the absence of a defining marker still expressed at postnatal stages, we characterized these cells by combining immunohistochemistry for Lhx1, which labels a mixed population, including V0, V1, and subsets of dorsal interneurons (dI4 and dIL$_A$), with FoxD3, which captures V1 interneurons (Pillai et al., 2007; Francius et al., 2013; Lu et al., 2015). In *afadin* $^{fl/fl}$ mice, we found an ectopic cluster of Lhx1^{+}/FoxD3^{-} neurons in the dorsal contralateral spinal cord (Figures 7A–7F and S6I). These cells are found in more lateral positions compared with the premotor Lbx1^{+} population, indicating that they might represent a different subtype (Figures 7G and 7H). We also examined the number and distribution of FoxD3^{+} premotor interneurons in *afadin* $^{fl/fl}$ mice, but we did not find any significant difference compared with control animals (Figures S6C–S6H). Next we analyzed V0c neurons, a subset of V0 neurons recognizable by their cholinergic character and position in lamina X (Zagoraiou et al., 2009). V0c neurons have been shown to affect the modulation of motor output and to bilaterally connect to motor neurons (Zagoraiou et al., 2009; Stepien et al., 2010). As expected, we observed contralaterally projecting V0c premotor neurons in control and *afadin* $^{fl/fl}$ mice (Figures 7I–7L). However, we found a significant increase in the percentage of contralateral V0c premotor neurons in mutant mice, whereas the number and distribution of the ipsilateral ones was not changed (Figures 7M and 7N). We next checked whether the position of V0c neurons was affected by the presence of a double central canal in *afadin* $^{fl/fl}$ mice, but we did not observe any significant difference in their positioning (Figures 7O, 7P, and S7A–S7D). Finally, we analyzed premotor connectivity of V2a interneurons, a population consisting of ipsilaterally projecting excitatory interneurons defined by Chx10 expression (Al-Mosawie et al., 2007; Lundfald et al., 2007). In control mice, we observed Chx10^{+} premotor interneurons exclusively in the ipsilateral side of the spinal cord (Figures 7Q and 7S). In contrast, contralateral Chx10^{+} premotor neurons were found in *afadin* $^{fl/fl}$ mice (Figures 7R and 7T–7V). Moreover, we did not observe any difference in the number or location of ipsilateral V2a premotor neurons or the general V2a population (Figures 7W, 7X, and S7E–S7H). Altogether, these data indicate ectopic contralateral connectivity in multiple cardinal interneuron subtypes in afadin mutant mice.

DISCUSSION

The precise rhythm and pattern of muscle activation underlie execution of coordinated movements and rely on correct assembly and function of spinal circuits. We found that conditional elimination of afadin in motor neuron progenitors results in loss

Figure 6. Aberrant Wiring of Premotor Circuits in Afadin Mutant Mice

(A and B) Transverse sections of a control (A) and an *afadin* $^{fl/fl}$ (B) spinal cords showing rabies-labeled interneurons.

(C and D) Digital reconstructions of interneuron positions after rabies injection in the extensor carpi radialis muscle of a control (C) and an *afadin* $^{fl/fl}$ (D) mouse.

(E) Average number of interneurons labeled in control and *afadin* $^{fl/fl}$ mice (mean ± SEM; t test, $p > 0.05$; n = 3).

(F) Dorso-ventral density analysis of contralateral interneurons in control and *afadin* $^{fl/fl}$ mice (n = 3).

(G and H) Transverse contour density plots of contralateral interneurons in control (G) and *afadin* $^{fl/fl}$ mice (H) (n = 3).

(I and J) Percentage of interneurons in the dorsal and ventral quadrant of the ipsilateral (I) and contralateral (J) sides of the spinal cords in control and *afadin* $^{fl/fl}$ mice (mean ± SEM; t test, * = $p < 0.05$; n = 3).

(K and L) Contralateral transverse sections of a control (K) and an *afadin* $^{fl/fl}$ (L) spinal cords showing rabies-labeled interneurons and Lbx1 expression. Insets show magnification of a representative neuron marked by the arrow.

(M and N) Digital reconstruction of rabies^{+}/Lbx1^{+} interneuron positions in control (M) and *afadin* $^{fl/fl}$ (N) mice (n = 3).

(O) Percentage of rabies^{+}/Lbx1^{+} interneurons in the contralateral dorsal and ventral quadrants of the spinal cord (mean ± SEM; t test, ** = $p < 0.01$; n = 3).

(P) Dorso-ventral density analysis of contralateral rabies^{+}/Lbx1^{+} interneurons in control and *afadin* $^{fl/fl}$ mice (n = 3).

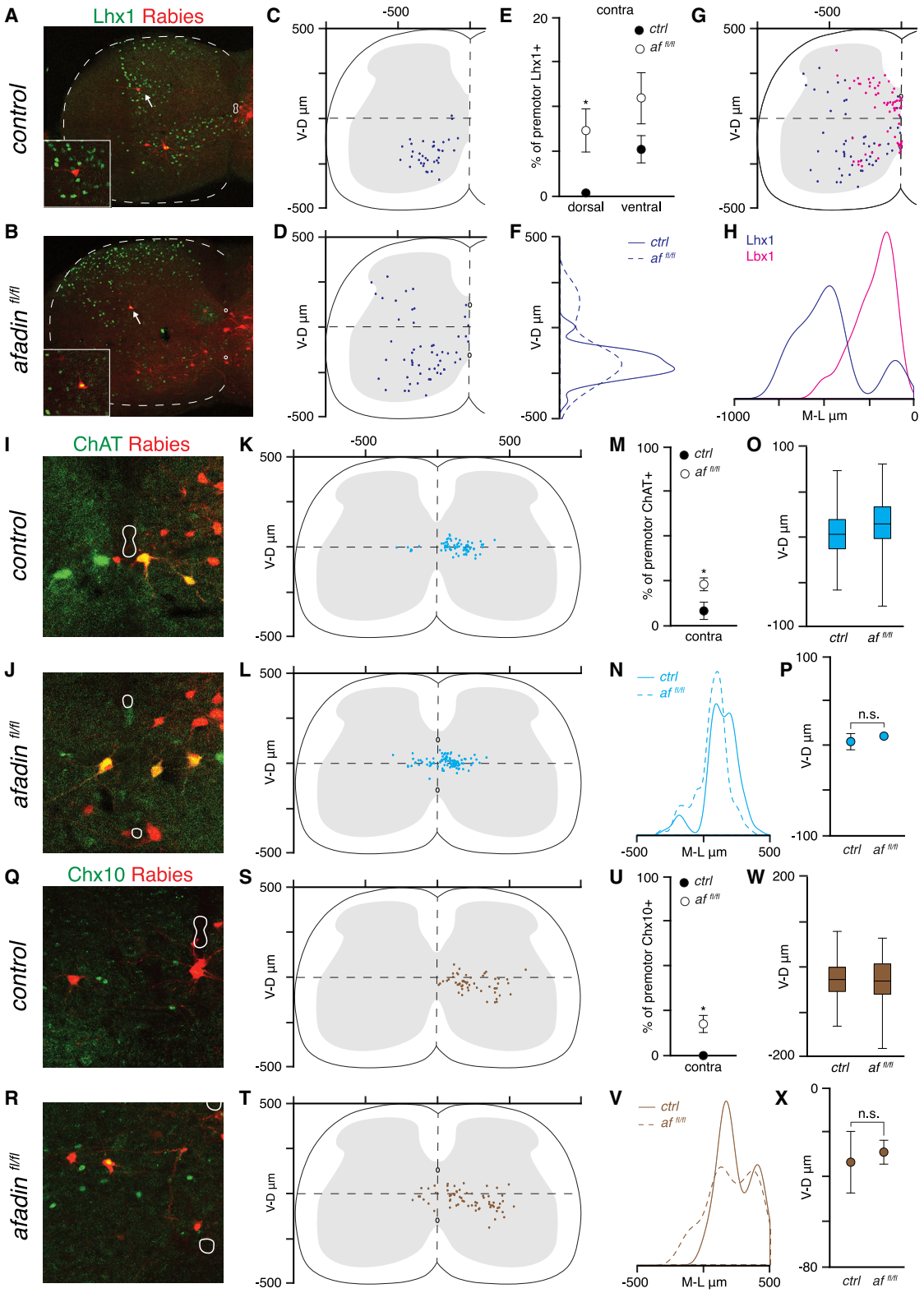

Figure 7. Multiple Interneuron Subtypes Are Miswired in Afadin Mutant Mice

(A and B) Contralateral transverse sections of a control (A) and an *afadin* $^{fl/fl}$ (B) spinal cords showing rabies-labeled interneurons and Lhx1 expression. Insets show magnification of a representative neuron marked by the arrow.

(legend continued on next page)

of left-right limb alternation in favor of synchronous movement. Our data show that afadin function at the neuroepithelium is important for lumen formation and that, in its absence, development of midline structures is perturbed. In particular, afadin elimination from the pMN results in a double central canal phenotype. As a consequence, the anatomical organization of the spinal midline is disrupted. Analysis of premotor circuit assembly shows the emergence of ectopic clusters of contralateral premotor interneurons in afadin mutant mice. In particular, our data indicate that miswiring of multiple subtypes, including dI4-5, V0, V0c, and V2a identities, is necessary to cause loss of left-right limb alternation.

Afadin Is a Key Regulator of Lumen Formation

Generation of tubular structures is a morphogenetic process essential for functional organization of many organs and relies on establishment of epithelial polarity and actin cytoskeleton remodeling (Datta et al., 2011). Afadin is known to have important roles in epithelial cells in the formation of adherens and tight junctions as well as in the organization of apicobasal polarity (Mandai et al., 2013). In the developing kidney and pancreas, afadin has been shown to be a central element in the generation and elongation of epithelial tubules. Lumen formation in the kidney requires alignment of apical membrane domains on adjacent epithelial cells that coalesce to generate a lumen, and, upon afadin elimination, nephrons develop a discontinuous lumen (Yang et al., 2013). Similarly, formation of uninterrupted pancreatic lumens occurs via apical membrane biogenesis in a highly coordinated process between epithelial cells that depends on afadin function (Azizoglu et al., 2017). Our findings in the spinal cord are in line with these observations. Elimination of afadin from the pMN creates a gap between adjoining neuroepithelial areas at the midline, precluding their coalescence and causing formation of two independent luminal structures. Moreover, elimination of afadin from dorsal progenitors expressing Wnt1 also perturbs organization of the midline and results in displacement of the central canal to a more ventral position, highlighting the important role of afadin along the whole dorso-ventral extent of the spinal neuroepithelium.

Lumen morphogenesis in the pancreas has been shown to rely on the cooperation of afadin and RhoA activities in the control of cytoskeletal remodeling (Azizoglu et al., 2017). In the spinal cord, previous work showed that elimination of RhoA from the neuroepithelium leads to defects in midline development, indicating that the same signaling pathway controls tubulogenesis in different organs and raising the question of whether specific cell surface receptors are required for this function (Katayama et al., 2012; Mulherkar et al., 2013). Afadin is known to support function of the classical cadherin and nectin families of adhesion molecules (Takai et al., 2008; Mandai et al., 2013). We showed that elimination of afadin in motor neuron progenitors does not affect classical cadherin localization and function (Dewitz et al., 2018). The nectin family consists of four members: nectin-1, nectin-2, and nectin-3 are expressed at the spinal neuroepithelium during development, whereas nectin-4 is not detectable (Okabe et al., 2004; Dewitz et al., 2018). We observed perturbation in nectin-1, nectin-2, and nectin-3 expression at the pMN upon elimination of afadin in motor neuron progenitors (data not shown). However, single nectin mutant mice do not present anatomical or locomotor phenotypes similar to the ones found after elimination of afadin (Takai et al., 2008; Mandai et al., 2015). These observations indicate that nectins may have a redundant function, upstream of afadin, in the control of neuroepithelial integrity in the spinal cord. Finally, afadin has also been implicated in control of the ephrin/Eph and Slit/Robo pathways, raising the possibility that multiple effectors could contribute to the phenotype (Hock et al., 1998; Slováková et al., 2012).

The Double Central Canal and Wiring of Spinal Motor Circuits

How does generation of a double central canal affect wiring of spinal motor circuits? Our data show that perturbation of central canal formation results in altered organization of the spinal cord midline. We found that ephrin B3, which is normally expressed along the entire dorso-ventral extent of the gray matter, is lost between the two canals, suggesting that the tissue in the central area of the spinal cord is not properly organized (Imondi et al., 2000; Kullander et al., 2001). Similarly, the extent of netrin 1 expression along the ventral half of the midline is also reduced (Serafini et al., 1996). Despite these

(C and D) Digital reconstructions of contralateral rabies$^+$/Lhx1$^+$ interneuron positions in control (C) and *afadin* $^{fl/fl}$ (D) mice (n = 3).
(E) Percentage of rabies$^+$/Lhx1$^+$ interneurons in the contralateral dorsal and ventral quadrants of the spinal cord (mean ± SEM; t test, *p < 0.05; n = 3).
(F) Dorso-ventral density analysis of contralateral rabies$^+$/Lhx1$^+$ interneurons in control and *afadin* $^{fl/fl}$ mice (n = 3).
(G) Digital reconstruction of contralateral rabies$^+$/Lhx1$^+$ (dark blue) and rabies$^+$/Lbx1$^+$ (magenta) interneuron positions in *afadin* $^{fl/fl}$ mice (n = 3).
(H) Medio-lateral density analysis in the contralateral dorsal quadrant of rabies$^+$/Lhx1$^+$ (dark blue) and rabies$^+$/Lbx1$^+$ (magenta) interneurons in *afadin* $^{fl/fl}$ mice (n = 3).
(I and J) Transverse spinal cord sections showing rabies-labeled interneurons and ChAT expression in the central canal area in control (I) and *afadin* $^{fl/fl}$ (J) mice.
(K and L) Digital reconstruction of rabies$^+$/ChAT$^+$ interneuron positions in control (K) and *afadin* $^{fl/fl}$ (L) mice (n = 3).
(M) Percentage of rabies$^+$/ChAT$^+$ interneurons in the contralateral side of the spinal cord (mean ± SEM; t test, *p < 0.05; n = 3).
(N) Medio-lateral density analysis of rabies$^+$/ChAT$^+$ interneurons in control and *afadin* $^{fl/fl}$ mice (n = 3).
(O) Boxplots showing distribution of rabies$^+$/ChAT$^+$ interneurons in control and *afadin* $^{fl/fl}$ mice along the dorso-ventral axis (n = 3).
(P) Average dorso-ventral position of rabies$^+$/ChAT$^+$ interneurons in control and *afadin* $^{fl/fl}$ mice (mean ± SEM; t test, p > 0.05; n = 3).
(Q and R) Transverse spinal cord sections showing rabies-labeled interneurons and Chx10 expression in the central canal area in control (Q) and *afadin* $^{fl/fl}$ (R) mice.
(S and T) Digital reconstruction of rabies$^+$/Chx10$^+$ interneuron positions in control (S) and *afadin* $^{fl/fl}$ (T) mice (n = 4).
(U) Percentage of rabies$^+$/Chx10$^+$ interneurons on the contralateral side of the spinal cord (mean ± SEM; t test, *p < 0.05; n = 4).
(V) Medio-lateral density analysis of rabies$^+$/Chx10$^+$ interneurons in control and *afadin* $^{fl/fl}$ mice (n = 4).
(W) Boxplots showing distribution of rabies$^+$/Chx10$^+$ interneurons in control and *afadin* $^{fl/fl}$ mice along the dorso-ventral axis (n = 4).
(X) Average dorso-ventral position of rabies$^+$/Chx10$^+$ interneurons in control and *afadin* $^{fl/fl}$ mice (mean ± SEM; t test, p > 0.05; n = 4).

remarkable anatomical defects, we did not observe any change in the stereotypic positioning of spinal interneurons normally residing in the intermediate zone of the spinal cord, indicating that the generation and migration of interneurons are not affected by formation of a double central canal. Thus, our data suggest that impairment in lumen morphogenesis compromises the organization of midline signals ensuring laterality in circuit wiring.

Connectivity Defects in Multiple Premotor Neuron Subtypes in Afadin Mutant Mice

Perturbation of the localization of midline cues controlling guidance of developing axons is predicted to affect laterality in wiring of motor circuits (Kullander et al., 2001; Rabe et al., 2009). Despite the reduction in the extent of netrin 1 expression in the ventral spinal cord in afadin mutant mice, we did not observe any obvious defect in commissural axon organization. Elimination of ephrin B3 expression between the two central canals in afadin mutant mice is predicted to open a way across the midline for EphA4-expressing axons during assembly of spinal circuits. It has been shown that perturbation of EphA4 signaling in interneurons derived from the Lbx1 progenitor domain results in aberrant contralateral projections (Paixão et al., 2013). Lbx1-derived interneurons can be divided into three main subpopulations: dI4 and dI5 neurons residing in the dorsal spinal cord and ventral dI6 neurons (Gross et al., 2002; Müller et al., 2002). In afadin mutant mice, we found Lbx1^{+} contralateral premotor neurons in the dorsal spinal cord, indicating a role of dI4-5 neurons in circuits controlling gait selection. The same population of interneurons has been identified as a source of ectopic contralateral projections to motor neurons in EphA4 knockout mice, and conditional elimination of EphA4 in Lbx1-derived interneurons is sufficient to result in connectivity defects (Satoh et al., 2016). These mice present an alternating gait during on-ground locomotion but conditionally switch to a synchronous gait when performing locomotor tasks demanding less weight load, such as swimming or air stepping. These observations suggest that changes in the connectivity of multiple interneurons subtypes are required to constitutively synchronize paired limb movement.

Our experiments with afadin mutant mice provide important clues for identification of additional defects in premotor connectivity required for a complete switch to synchrony. We found an ectopic premotor cluster of Lhx1^{+}/FoxD3^{-} neurons in the dorsal contralateral spinal cord. These cells reside in a more lateral position compared to the Lbx1^{+} cluster, indicating that they constitute a different subset of Lbx1-derived neurons or may originate from V0 progenitors (Lu et al., 2015). Interestingly, we did not observe any difference in premotor connectivity of neurons labeled by FoxD3, which comprise mostly V1 inhibitory interneurons that have no described role in left-right alternation (Arber, 2012). A fraction of V0 neurons has been shown to express EphA4 during embryonic development; however, no defects in connectivity across the midline for V0 neurons in mice with perturbed ephrin signaling have been reported yet (Lundfald et al., 2007). We observed an increase in contralateral connectivity of V0c neurons, a small cholinergic subset of V0 neurons that has been shown to bilaterally connect to motor neurons and participate in modulation of motor output (Zagoraiou et al., 2009; Stepien et al., 2010). Thus, our data suggest that incorrect wiring of V0c could also contribute to the deregulation of circuits controlling gait choice. Finally, we found ectopic contralateral premotor neurons characterized by expression of Chx10. V2a neurons are predicted to be a main culprit for the loss of left-right alternation in the absence of ephrin signaling because of their exclusive ipsilateral connectivity, glutamatergic character, and expression of EphA4 (Al-Mosawie et al., 2007; Lundfald et al., 2007; Borgius et al., 2014). Moreover, genetic ablation of V2a neurons results in loss of left-right alternation in a speed-dependent manner (Crone et al., 2009). However, contralaterally projecting V2a neurons have not been observed previously in EphA4-null mice (Lundfald et al., 2007). In contrast, our data also show that laterality in V2a neuron connectivity is compromised in the absence of ephrin signaling and suggest that this defect contributes to the constitutive emergence of a bound gait.

STAR★METHODS

Detailed methods are provided in the online version of this paper and include the following:

- KEY RESOURCES TABLE
- RESOURCE AVAILABILITY
  - Lead Contact
  - Materials Availability
  - Data and Code Availability
- EXPERIMENTAL MODEL AND SUBJECT DETAILS
  - Animal Experimentation Ethical Approval
  - Animal models
- METHOD DETAILS
  - Gait analysis
  - Isolated spinal cord preparations
  - Analysis of fictive locomotion data
  - Rabies virus production
  - Intramuscular injections
  - Perfusion
  - Dissection and tissue processing
  - Contralateral interneurons tracing
  - Immunohistochemistry
  - *In situ* hybridization
  - Three-dimensional positional analysis
- QUANTIFICATION AND STATISTICAL ANALYSIS

SUPPLEMENTAL INFORMATION

Supplemental Information can be found online at https://doi.org/10.1016/j.celrep.2020.107741.

ACKNOWLEDGMENTS

We thank Liana Kosizki, Isabelle Werner, and Aurélie Heuzé for technical support and the MDC Advanced Light Microscope Facility for assistance with image acquisition and analysis. We are grateful to Carmen Birchmeier for the gift of the Lbx1 and FoxD3 antibodies. The Lhx1 antibody was a gift from Susan

Morton. Dario Bonanomi provided the probe against netrin-1. We thank Marco Beato, Stephan Dietrich, Katrin Gerstmann, and Sofia Pimpinella for valuable discussions and comments on the manuscript. S.S. and N.Z. were supported by the DFG (ZA 885/1-1 and EXC 257 NeuroCure) and J.B. by ANR grant ANR-17-CE16-0027.

AUTHOR CONTRIBUTIONS

Conceptualization, S.S. and N.Z.; Investigation, S.S., C.H., and E.T.; Formal Analysis, S.S, C.S.M., and J.B.; Writing – Original Draft, S.S. and N.Z.; Writing – Review and Editing, S.S., J.B. and N.Z.; Supervision, J.B. and N.Z.

DECLARATION OF INTERESTS

The authors declare no competing interests.

Received: June 28, 2019
Revised: April 3, 2020
Accepted: May 15, 2020
Published: June 9, 2020; corrected online January 6, 2021

REFERENCES

Al-Mosawie, A., Wilson, J.M., and Brownstone, R.M. (2007). Heterogeneity of V2-derived interneurons in the adult mouse spinal cord. Eur. J. Neurosci. *26*, 3003–3015.

Arber, S. (2012). Motor circuits in action: specification, connectivity, and function. Neuron *74*, 975–989.

Azizoglu, D.B., Braitsch, C., Marciano, D.K., and Cleaver, O. (2017). Afadin and RhoA control pancreatic endocrine mass via lumen morphogenesis. Genes Dev. *31*, 2376–2390.

Beaudoin, G.M.J., 3rd, Schofield, C.M., Nuwal, T., Zang, K., Ullian, E.M., Huang, B., and Reichardt, L.F. (2012). Afadin, a Ras/Rap effector that controls cadherin function, promotes spine and excitatory synapse density in the hippocampus. J. Neurosci. *32*, 99–110.

Beg, A.A., Sommer, J.E., Martin, J.H., and Scheiffele, P. (2007). α2-Chimaerin is an essential EphA4 effector in the assembly of neuronal locomotor circuits. Neuron *55*, 768–778.

Bellardita, C., and Kiehn, O. (2015). Phenotypic characterization of speed-associated gait changes in mice reveals modular organization of locomotor networks. Curr. Biol. *25*, 1426–1436.

Bikoff, J.B., Gabitto, M.I., Rivard, A.F., Drobac, E., Machado, T.A., Miri, A., Brenner-Morton, S., Famojure, E., Diaz, C., Alvarez, F.J., et al. (2016). Spinal Inhibitory Interneuron Diversity Delineates Variant Motor Microcircuits. Cell *165*, 207–219.

Borgius, L., Nishimaru, H., Caldeira, V., Kunugise, Y., Löw, P., Reig, R., Itohara, S., Iwasato, T., and Kiehn, O. (2014). Spinal glutamatergic neurons defined by EphA4 signaling are essential components of normal locomotor circuits. J. Neurosci. *34*, 3841–3853.

Chédotal, A. (2019). Roles of axon guidance molecules in neuronal wiring in the developing spinal cord. Nat. Rev. Neurosci. *20*, 380–396.

Crone, S.A., Quinlan, K.A., Zagoraiou, L., Droho, S., Restrepo, C.E., Lundfald, L., Endo, T., Setlak, J., Jessell, T.M., Kiehn, O., and Sharma, K. (2008). Genetic ablation of V2a ipsilateral interneurons disrupts left-right locomotor coordination in mammalian spinal cord. Neuron *60*, 70–83.

Crone, S.A., Zhong, G., Harris-Warrick, R., and Sharma, K. (2009). In mice lacking V2a interneurons, gait depends on speed of locomotion. J. Neurosci. *29*, 7098–7109.

Dasen, J.S., Tice, B.C., Brenner-Morton, S., and Jessell, T.M. (2005). A Hox regulatory network establishes motor neuron pool identity and target-muscle connectivity. Cell *123*, 477–491.

Datta, A., Bryant, D.M., and Mostov, K.E. (2011). Molecular regulation of lumen morphogenesis. Curr. Biol. *21*, R126–R136.

Demireva, E.Y., Shapiro, L., Jessell, T.M., and Zampieri, N. (2011). Motor Neuron Position and Topographic Order Imposed by β- and γ-Catenin Activities. Cell *147*, 641–652.

Dessaud, E., Yang, L.L., Hill, K., Cox, B., Ulloa, F., Ribeiro, A., Mynett, A., Novitch, B.G., and Briscoe, J. (2007). Interpretation of the sonic hedgehog morphogen gradient by a temporal adaptation mechanism. Nature *450*, 717–720.

Dewitz, C., Pimpinella, S., Hackel, P., Akalin, A., Jessell, T.M., and Zampieri, N. (2018). Nuclear Organization in the Spinal Cord Depends on Motor Neuron Lamination Orchestrated by Catenin and Afadin Function. Cell Rep. *22*, 1681–1694.

Francius, C., Harris, A., Rucchin, V., Hendricks, T.J., Stam, F.J., Barber, M., Kurek, D., Grosveld, F.G., Pierani, A., Goulding, M., and Clotman, F. (2013). Identification of multiple subsets of ventral interneurons and differential distribution along the rostrocaudal axis of the developing spinal cord. PLoS ONE *8*, e70325.

Gil-Sanz, C., Landeira, B., Ramos, C., Costa, M.R., and Müller, U. (2014). Proliferative defects and formation of a double cortex in mice lacking Mltt4 and Cdh2 in the dorsal telencephalon. J. Neurosci. *34*, 10475–10487.

Gosgnach, S., Bikoff, J.B., Dougherty, K.J., El Manira, A., Lanuza, G.M., and Zhang, Y. (2017). Delineating the Diversity of Spinal Interneurons in Locomotor Circuits. J. Neurosci. *37*, 10835–10841.

Goulding, M. (2009). Circuits controlling vertebrate locomotion: moving in a new direction. Nat. Rev. Neurosci. *10*, 507–518.

Grillner, S. (2006). Biological pattern generation: the cellular and computational logic of networks in motion. Neuron *52*, 751–766.

Grillner, S., and Jessell, T.M. (2009). Measured motion: searching for simplicity in spinal locomotor networks. Curr. Opin. Neurobiol. *19*, 572–586.

Gross, M.K., Dottori, M., and Goulding, M. (2002). Lbx1 specifies somatosensory association interneurons in the dorsal spinal cord. Neuron *34*, 535–549.

Hock, B., Böhme, B., Karn, T., Yamamoto, T., Kaibuchi, K., Holtrich, U., Holland, S., Pawson, T., Rübsamen-Waigmann, H., and Strebhardt, K. (1998). PDZ-domain-mediated interaction of the Eph-related receptor tyrosine kinase EphB3 and the ras-binding protein AF6 depends on the kinase activity of the receptor. Proc. Natl. Acad. Sci. USA *95*, 9779–9784.

Imondi, R., Wideman, C., and Kaprielian, Z. (2000). Complementary expression of transmembrane ephrins and their receptors in the mouse spinal cord: a possible role in constraining the orientation of longitudinally projecting axons. Development *127*, 1397–1410.

Iwasato, T., Katoh, H., Nishimaru, H., Ishikawa, Y., Inoue, H., Saito, Y.M., Ando, R., Iwama, M., Takahashi, R., Negishi, M., and Itohara, S. (2007). Rac-GAP α-chimerin regulates motor-circuit formation as a key mediator of EphrinB3/EphA4 forward signaling. Cell *130*, 742–753.

Katayama, K., Leslie, J.R., Lang, R.A., Zheng, Y., and Yoshida, Y. (2012). Left-right locomotor circuitry depends on RhoA-driven organization of the neuroepithelium in the developing spinal cord. J. Neurosci. *32*, 10396–10407.

Kiehn, O. (2006). Locomotor circuits in the mammalian spinal cord. Annu. Rev. Neurosci. *29*, 279–306.

Kiehn, O. (2016). Decoding the organization of spinal circuits that control locomotion. Nat. Rev. Neurosci. *17*, 224–238.

Kjaerulff, O., and Kiehn, O. (1996). Distribution of networks generating and coordinating locomotor activity in the neonatal rat spinal cord in vitro: a lesion study. J. Neurosci. *16*, 5777–5794.

Kullander, K., Croll, S.D., Zimmer, M., Pan, L., McClain, J., Hughes, V., Zabski, S., DeChiara, T.M., Klein, R., Yancopoulos, G.D., and Gale, N.W. (2001). Ephrin-B3 is the midline barrier that prevents corticospinal tract axons from recrossing, allowing for unilateral motor control. Genes Dev. *15*, 877–888.

Kullander, K., Butt, S.J.B., Lebret, J.M., Lundfald, L., Restrepo, C.E., Rydström, A., Klein, R., and Kiehn, O. (2003). Role of EphA4 and EphrinB3 in local neuronal circuits that control walking. Science *299*, 1889–1892.

Lanuza, G.M., Gosgnach, S., Pierani, A., Jessell, T.M., and Goulding, M. (2004). Genetic identification of spinal interneurons that coordinate left-right locomotor activity necessary for walking movements. Neuron *42*, 375–386.

Lemieux, M., Josset, N., Roussel, M., Couraud, S., and Bretzner, F. (2016). Speed-dependent modulation of the locomotor behavior in adult mice reveals attractor and transitional gaits. Front. Neurosci. *10*, 42.

Lu, D.C., Niu, T., and Alaynick, W.A. (2015). Molecular and cellular development of spinal cord locomotor circuitry. Front. Mol. Neurosci. *8*, 25.

Lundfald, L., Restrepo, C.E., Butt, S.J.B., Peng, C.Y., Droho, S., Endo, T., Zeilhofer, H.U., Sharma, K., and Kiehn, O. (2007). Phenotype of V2-derived interneurons and their relationship to the axon guidance molecule EphA4 in the developing mouse spinal cord. Eur. J. Neurosci. *26*, 2989–3002.

Mandai, K., Rikitake, Y., Shimono, Y., and Takai, Y. (2013). Afadin/AF-6 and canoe: roles in cell adhesion and beyond. Prog. Mol. Biol. Transl. Sci. *116*, 433–454.

McHanwell, S., and Biscoe, T.J. (1981). The sizes of motoneurons supplying hindlimb muscles in the mouse. Proc. R. Soc. Lond. B Biol. Sci. *213*, 201–216.

Mendes, C.S., Bartos, I., Márka, Z., Akay, T., Márka, S., and Mann, R.S. (2015). Quantification of gait parameters in freely walking rodents. BMC Biol. *13*, 50.

Mulherkar, S., Liu, F., Chen, Q., Narayanan, A., Couvillon, A.D., Shine, H.D., and Tolias, K.F. (2013). The small GTPase RhoA is required for proper locomotor circuit assembly. PLoS ONE *8*, e67015.

Müller, T., Brohmann, H., Pierani, A., Heppenstall, P.A., Lewin, G.R., Jessell, T.M., and Birchmeier, C. (2002). The homeodomain factor lbx1 distinguishes two major programs of neuronal differentiation in the dorsal spinal cord. Neuron *34*, 551–562.

Müller, T., Anlag, K., Wildner, H., Britsch, S., Treier, M., and Birchmeier, C. (2005). The bHLH factor Olig3 coordinates the specification of dorsal neurons in the spinal cord. Genes Dev. *19*, 733–743.

Okabe, N., Shimizu, K., Ozaki-Kuroda, K., Nakanishi, H., Morimoto, K., Takeuchi, M., Katsumaru, H., Murakami, F., and Takai, Y. (2004). Contacts between the commissural axons and the floor plate cells are mediated by nectins. Dev. Biol. *273*, 244–256.

Osakada, F., and Callaway, E.M. (2013). Design and generation of recombinant rabies virus vectors. Nat. Protoc. *8*, 1583–1601.

Paixão, S., Balijepalli, A., Serradj, N., Niu, J., Luo, W., Martin, J.H., and Klein, R. (2013). EphrinB3/EphA4-mediated guidance of ascending and descending spinal tracts. Neuron *80*, 1407–1420.

Pillai, A., Mansouri, A., Behringer, R., Westphal, H., and Goulding, M. (2007). Lhx1 and Lhx5 maintain the inhibitory-neurotransmitter status of interneurons in the dorsal spinal cord. Development *134*, 357–366.

Rabe, N., Gezelius, H., Vallstedt, A., Memic, F., and Kullander, K. (2009). Netrin-1-dependent spinal interneuron subtypes are required for the formation of left-right alternating locomotor circuitry. J. Neurosci. *29*, 15642–15649.

Rossi, J., Balthasar, N., Olson, D., Scott, M., Berglund, E., Lee, C.E., Choi, M.J., Lauzon, D., Lowell, B.B., and Elmquist, J.K. (2011). Melanocortin-4 receptors expressed by cholinergic neurons regulate energy balance and glucose homeostasis. Cell Metab. *13*, 195–204.

Rowitch, D.H., S-Jacques, B., Lee, S.M.K., Flax, J.D., Snyder, E.Y., and McMahon, A.P. (1999). Sonic hedgehog regulates proliferation and inhibits differentiation of CNS precursor cells. J. Neurosci. *19*, 8954–8965.

Satoh, D., Pudenz, C., and Arber, S. (2016). Context-Dependent Gait Choice Elicited by EphA4 Mutation in Lbx1 Spinal Interneurons. Neuron *89*, 1046–1058.

Serafini, T., Colamarino, S.A., Leonardo, E.D., Wang, H., Beddington, R., Skarnes, W.C., and Tessier-Lavigne, M. (1996). Netrin-1 is required for commissural axon guidance in the developing vertebrate nervous system. Cell *87*, 1001–1014.

Slováková, J., Speicher, S., Sánchez-Soriano, N., Prokop, A., and Carmena, A. (2012). The actin-binding protein Canoe/AF-6 forms a complex with Robo and is required for Slit-Robo signaling during axon pathfinding at the CNS midline. J. Neurosci. *32*, 10035–10044.

Stepien, A.E., Tripodi, M., and Arber, S. (2010). Monosynaptic rabies virus reveals premotor network organization and synaptic specificity of cholinergic partition cells. Neuron *68*, 456–472.

Sürmeli, G., Akay, T., Ippolito, G.C., Tucker, P.W., and Jessell, T.M. (2011). Patterns of spinal sensory-motor connectivity prescribed by a dorsoventral positional template. Cell *147*, 653–665.

Takai, Y., Ikeda, W., Ogita, H., and Rikitake, Y. (2008). The Immunoglobulin-Like Cell Adhesion Molecule Nectin and Its Associated Protein Afadin. Annual Review of Cell and Developmental Biology *24*, 309–342.

Takatoh, J., Nelson, A., Zhou, X., Bolton, M.M., Ehlers, M.D., Arenkiel, B.R., Mooney, R., and Wang, F. (2013). New modules are added to vibrissal premotor circuitry with the emergence of exploratory whisking. Neuron *77*, 346–360.

Talpalar, A.E., Endo, T., Löw, P., Borgius, L., Hägglund, M., Dougherty, K.J., Ryge, J., Hnasko, T.S., and Kiehn, O. (2011). Identification of Minimal Neuronal Networks Involved in Flexor-Extensor Alternation in the Mammalian Spinal Cord. Neuron *71*, 1071–1084.

Talpalar, A.E., Bouvier, J., Borgius, L., Fortin, G., Pierani, A., and Kiehn, O. (2013). Dual-mode operation of neuronal networks involved in left-right alternation. Nature *500*, 85–88.

Wickersham, I.R., Lyon, D.C., Barnard, R.J.O., Mori, T., Finke, S., Conzelmann, K.-K., Young, J.A., and Callaway, E.M. (2007). Monosynaptic restriction of transsynaptic tracing from single, genetically targeted neurons. Neuron *53*, 639–647.

Yang, Z., Zimmerman, S., Brakeman, P.R., Beaudoin, G.M., 3rd, Reichardt, L.F., and Marciano, D.K. (2013). De novo lumen formation and elongation in the developing nephron: a central role for afadin in apical polarity. Development *140*, 1774–1784.

Zagoraiou, L., Akay, T., Martin, J.F., Brownstone, R.M., Jessell, T.M., and Miles, G.B. (2009). A cluster of cholinergic premotor interneurons modulates mouse locomotor activity. Neuron *64*, 645–662.

Zhang, Y., Narayan, S., Geiman, E., Lanuza, G.M., Velasquez, T., Shanks, B., Akay, T., Dyck, J., Pearson, K., Gosgnach, S., et al. (2008). V3 spinal neurons establish a robust and balanced locomotor rhythm during walking. Neuron *60*, 84–96.

Ziskind-Conhaim, L., and Hochman, S. (2017). Diversity of molecularly defined spinal interneurons engaged in mammalian locomotor pattern generation. J. Neurophysiol. *118*, 2956–2974.

STAR★METHODS

KEY RESOURCES TABLE

REAGENT or RESOURCE	SOURCE	IDENTIFIER
Antibodies		
anti-afadin antibody (guinea pig)	Dewitz et al., 2018	N/A
anti-ChAT antibody (rabbit)	Sürmeli et al., 2011	RRID:AB_2750952
anti-Chx10 antibody (sheep)	Abcam	RRID:AB_302278
anti-FoxD3 antibody (guinea pig)	Müller et al., 2005	N/A
anti-Hb9 antibody (rabbit)	Generated in Jessell laboratory	N/A
anti-Isl1/2 antibody (guinea pig)	Dasen et al., 2005	RRID:AB_2801512
anti-Lbx1 antibody (rabbit)	Müller et al., 2002	N/A
anti-Lhx1 antibody (rabbit)	Generated in the Jessell laboratory	RRID:AB_2827967
anti-ROBO3 antibody (goat)	R&D Systems	RRID:AB_2181865
anti-TAG1 antibody (goat)	R&D Systems	RRID:AB_2044647
Phalloidin-FITC	Sigma Aldrich	Cat #: P5282
NeuroTrace 640/660 Deep Red Fluorescent Nissl Stain antibody	Thermo Fisher	RRID:AB_2572212
Bacterial and Virus Strains		
Rabies virus-ΔG-mCherry	Generated in the Zampieri laboratory	N/A
Experimental Models: Cell Lines		
BHK B7GG	Osakada and Callaway, 2013	N/A
HEK293T	American Type Culture Collection	Cat #: CRL-3216
Experimental Models: Organisms/Strains		
Afdn $^{tm1.1Lfr}$	Beaudoin et al., 2012	MGI:5308214
Olig2$^{tm1(cre)Tmj}$	Dessaud et al., 2007	MGI:3774124
H2az2 $^{Tg(Wnt1-cre)11Rth}$	Rowitch et al., 1999	MGI:2386570
Chat $^{tm1(cre)Lowl}$	Rossi et al., 2011	MGI:3699161
Gt(Rosa)26Sor $^{tm1(CAG-RABVgp4,-TVA)Arenk}$	Takatoh et al., 2013	MGI:5550559
Oligonucleotides		
Netrin 1 *In situ* hybridization probe fw primer: CGT GAA CAT CAT CTC CGT GT	Eurofins Scientific	N/A
Netrin 1 *In situ* hybridization probe rev primer: GCA GTG GAG ACC AAA GCT G	Eurofins Scientific	N/A
Ephrin B3 *In situ* hybridization probe fw primer: GTT AGG TTT TGC GGG GCT	Eurofins Scientific	N/A
Ephrin B3 *In situ* hybridization probe fw primer: TTC CTA GCT CCC CAG GCT	Eurofins Scientific	N/A
Software and Algorithms		
MouseWalker	Mendes et al., 2015	N/A
R	R Development Core Team (2008)	RRID:SCR_000432

RESOURCE AVAILABILITY

Lead Contact

Further information and requests for resources and reagents should be directed to and will be fulfilled by the Lead Contact, Niccolò Zampieri (niccolo.zampieri@mdc-berlin.de).

Materials Availability

All unique reagents generated in this study are available from the Lead Contact without restriction.

Data and Code Availability

Original datasets supporting the current study are available from the Lead Contact upon request. This study did not generate any new code.

EXPERIMENTAL MODEL AND SUBJECT DETAILS

Animal Experimentation Ethical Approval

All experiments were performed in compliance with the German Animal Welfare Act and approved by the Regional Office for Health and Social Affairs Berlin (LAGeSo) under license numbers G0121/15 and G0122/15.

Animal models

Mice were bred under standard husbandry and housing conditions. The mouse lines were used in this study maintained on a C57B6/J background: *Olig2::Cre* (Dessaud et al., 2007), *ChAT::Cre* (Rossi et al., 2011), *Wnt1::Cre* (Rowitch et al., 1999), *afadin* ^{fl} (Beaudoin et al., 2012) and *RΦGT* (Takatoh et al., 2013). *afadin* ^{fl} and *RΦGT* were kept homozygous whereas all Cre-lines were kept heterozygous. Animals of both sexes were used interchangeably and we did not anticipate nor observe any influence to the outcome. Following ages were used in this study: *Afadin* $^{fl/fl}$*; Olig2Cre* $^{+/-}$ (E10.5-P63. These mice sporadically develop hydrocephalus. Mice with hydrocephalus were sacrificed as soon as the disease was diagnosed); *afadin* $^{fl/fl}$*; Wnt1Cre* $^{+/-}$ (E13.5-E16.5. These mice display exencephaly); *afadin* $^{fl/fl}$*; ChATCre* $^{+/-}$ (E10.5-P21); *afadin* $^{fl/fl}$*; Olig2Cre* $^{+/-}$; *RΦGT* $^{fl/+}$ (P4-P10. These mice sporadically develop hydrocephalus. Mice with hydrocephalus were euthanised as soon as the disease was diagnosed).

METHOD DETAILS

Gait analysis

Quantitative gait analysis was performed as previously described (Mendes et al., 2015). Briefly, a customized acrylic glass walkway was constructed and surrounded by LED lights to generate the frustrated total internal reflection effect that is at the basis of the optical touch sensor that tracks the footprints. A lightbox was positioned above the walkway to visualize the body outline of the animals and a mirror was placed at a 45° angle below the walkway to reflect the signal to a high-speed camera. Before data acquisition, animals were habituated to the walkway setup and trained to walk straight from end to end. Three control animals and a total of nine *afadin* $^{fl/fl}$ mutant mice were analyzed. For each subject, three representative videos with uninterrupted runs at similar velocities were evaluated using the customized open-source MouseWalker software and the quantifiable parameters averaged.

Isolated spinal cord preparations

Postnatal days 0-3 mice were used in all experiments. The pups were anesthetized with isoflurane, decerebrated and the spinal cord was dissected and isolated in ice-cold Ringer's solution that contained (in mM): 111 NaCl, 3 KCl, 25 $NaHCO_3$, 1.25 $MgSO_4$, 1.1 KH_2PO_4, 2.5 $CaCl_2$ and 11 D-Glucose, and oxygenated in 95% O_2, 5%CO_2 to obtain a pH of 7.4. Isolated spinal cords (from T8 to S1) were transferred into a recording chamber that was continuously perfused with the above Ringer's solution, and pinned to a Sylgard 184 resin. All recordings were done at room temperature (22-25°C). Drug-evoked locomotor-like activities were induced by bath-applying 7-10 μM of N-methyl-D-aspartate (NMDA, Tocris) and 8-10 μM of serotonin (5-HT, Sigma-Aldrich). Neuronal activities were recorded using extracellular suction glass pipettes (120F-10, Harvard Apparatus) attached to the 2nd and 5th lumbar ventral root (rL2, lL2, rL5). Signals were collected and band-passed filtered at 100 Hz to 1 kHz with an AC amplifier (Model 1700, A-M Systems) and live-integrated (Neurolog, Digitimer) with a time constant of 200 ms. Signals were sampled using Clampex 11 (Molecular Devices) at 5 kHz.

Analysis of fictive locomotion data

For each preparation, flexor-extensor coordination was analyzed offline for 40 consecutive locomotor bursts, taken after the locomotor activity had stabilized, i.e., 15-20 min after the initial burst of activity, as previously described (Talpalar et al., 2013). The left 2nd lumbar root was taken as a reference and bursts timings were detected manually using Clampfit (Molecular Devices). The cycle periods of this reference trace were normalized to a scale from 0 to 1, with the onset of a locomotor burst corresponding to a phase value of 0 and the onset of the next burst corresponding to a phase value of 1. The onset of the burst on the contralateral root (lL2) was normalized to this reference cycle and expressed as a fraction from 0 to 1. This value was used to illustrate the L/R phase in figures, produce distribution histograms, or plotted on circular plots (Kjaerulff and Kiehn, 1996; Talpalar et al., 2011). For each preparation, the preferred mean phase of the activity was calculated. The direction of the corresponding vector gives the preferred phase of the activity and the length of the vector the precision of the phase [upper half circle: synchrony, lower half circle: alternation; (Kjaerulff and Kiehn, 1996; Talpalar et al., 2011). P values smaller than 0.05 determined by Rayleigh's test and represented outside of the inner circle, were considered significant.

Rabies virus production

Production of rabies virus was performed as previously described (Osakada and Callaway, 2013). Briefly, rabies virus production was started by infecting one T175 flask of BHK B7GG cells with stocks of rabies virusΔG-mCherry (RVΔG-mCherry) supernatant with a titer of at least 10^6 virus particles/ml. Cells were kept at 35°C and 3% CO_2 and medium was collected after four and seven days, centrifuged at 1000 rpm for 5 minutes and filtered. Amplification was started by infecting ten T175 flasks of BHK B7GG cells with the filtered starter culture. Medium was collected after four, seven and ten days, centrifuged at 1000 rpm for 5 minutes and filtered. To concentrate the virus, the medium was centrifuged at 24000 rpm for 2 hours. Pellets were resuspended in 400 μL Hanks' balanced salt solution (HBSS), tubes were covered with parafilm and incubated ON on a shaker at 4°C. Resuspended pellets were pooled and concentrated at 4°C using an Amicon Ultra 4 mL Filter (Merck Millipore) until a volume of approximately 100 μL was reached. Virus suspension was aliquoted and stored at −80°C until further use. Titer was determined by infecting HEK293T with serial dilutions of virus suspension.

Intramuscular injections

For motor pools analysis at adult stages, p60 animals were injected subcutaneously with 5 mg of carprofen per kg of weight as pre-emptive analgesia 30 minutes prior to surgery. Animals were then initially anesthetized with 4% isoflurane and checked for the toe pinch reflex before any procedure was done. Once sedated, they were placed on top of a circulating warm water blanket maintained at 37°C while keeping them under the effect of 2% isoflurane. Eye lubricant was applied to prevent their eyes from drying out. Head and body were gently fixed with tape to minimize movement during the surgery. To avoid any infection during the procedure, the hindlimbs were treated with iodine solution. A small incision was made in the skin to reveal the gastrocnemius (GS) and tibialis anterior (TA) muscles and a glass capillary was used to introduce 1 μL of cholera toxin subunit B (CTB) conjugated to either Alexa Fluor 488 or 555 (Thermo Fisher). Following injection, the skin was sutured with a nylon surgical suture. Animals were sacrificed three days post-surgery.

For monosynaptic tracing analysis P4 animals were anesthetized as described above and injected with 1.5 μL of RVΔG-mCherry in the extensor carpis radialis (ECR) muscle. Animals were sacrificed six days post-surgery.

Perfusion

Animals were anesthetized by intraperitoneal injection of 0.1 mL ketamine /xylazine mix per 10 g of weight (final concentrations: 120 mg/kg and 10 mg/kg, respectively) and checked for toe-pinch reflex before any procedure was done. Animals were first transcardially perfused with ice-cold PBS until the liver was cleared of blood, followed by freshly made ice-cold 4% PFA until no tremors could be observed anymore. Amount of PBS and PFA needed for a complete fixation depended on the age and weight of the animal (approximately 6 mL of each solution were used for neonates and 12-15 mL for adult animals).

Dissection and tissue processing

Spinal cords were dissected by decapitating the animals, opening up the belly and rib cage and removing the visceral organs. For all animals older than E13.5, ventral laminectomy was performed to allow better penetration of the fixative solution. Spinal cords were fixed for 90 minutes in 4% PFA on ice. This was followed by three washes with ice-cold PBS for 5 minutes each and over night incubation in 30% sucrose in 0.1M PB at 4°C for cryoprotection. Samples were embedded in Optimal Cutting Temperature (O.C.T., TissueTek) compound, frozen on dry ice and stored at −80°C.

Contralateral interneurons tracing

E15.5 embryos were dissected as described above. 0.5 μL of 1% tetramethylrhodamine-dextran solution was injected unilaterally with a glass capillary in the spinal cord between C5 and C8. Injected embryos were incubated in oxygenated 1x ACSF (127 mM NaCl; 3 mM KCl; 1.25 mM NaH_2PO_4 * 2 H_2O; 26 mM $NaHCO_3$; 10 mM glucose; 2 mM $CaCl_2$; 1 mM $MgCl_2$) over night at room temperature, followed by 5 hours of fixation in 4% PFA at 4°C. Embryos were subsequently processed as described above.

Immunohistochemistry

16 μm or 40 μm spinal cord cryosections were acquired with a Leica cryostat and collected on superfrost microscope slide. Slides were kept at room temperature for approximately 30 minutes to ensure good adhesion of the tissue on the glass. Sections were then first rehydrated with PBS for 10 minutes before adding freshly prepared dilutions of primary antibodies in 0.1% Triton X-100 in PBS (PBX, 16 μm) or 0.3% PBX (40 μm) for over night incubation at 4°C. Primary antibody dilutions were used as follows: guinea pig anti-afadin 1/20000, rabbit anti-ChAT 1/16000, sheep anti-Chx10 1/500, guinea pig anti-FoxD3 1/20000, rabbit anti-Hb9 1/8000, guinea pig anti-Isl1 1/30000, rabbit anti-Lbx1 1/10000, rabbit anti-Lhx1 1/10000, goat anti-ROBO3 1/200, goat anti-TAG1 1/200. After three washes with 0.1% PBX for 5 min each, secondary antibodies diluted in 0.1% or 0.3% PBX were added for 1 hour at room temperature. Alexa Fluor 488- and Cy3-conjugated secondary antibodies were used at 1/1000, Cy5-conjugated secondary antibodies at 1/500. Sections were then washed twice with 0.1% PBX for 5 minutes, followed by a final wash with PBS for 10 minutes. Slides were mounted with Vectashield (Vector). Nissl and phalloidin stainings were performed by adding NeuroTrace (Thermo Fisher) at 1/250 or Phalloidin-FITC (Sigma Aldrich) at 1/2000 along with the secondary antibodies.

In situ hybridization

In situ hybridization histochemistry was performed on 12 μm cryosections using digoxigenin (DIG)-labeled cRNA probes. DNA templates for mouse ephrin B3 and netrin 1 were cloned from cDNAs into pBluescript II SK^+ vector. Antisense DIG-cRNA probes were generated from DNA templates by RT-PCR using a DIG RNA Labeling Kit (Roche).

In situ hybridization was performed as previously described (Demireva et al., 2011). Briefly, slides were treated as follows: air-dried for 30 minutes, fixed with freshly made 4% PFA for 10 minutes, washed with PBS three times, treated with Proteinase K at 1mg/ml for 5 minutes, fixed with 4% PFA for 5 minutes, washed with PBS three times, acetylated for 10 minutes in 1.25% triethanolamine; 0.25% acetic acid anhydride; 0.175% HCl, washed with PBS three times and equilibrated with hybridization buffer (50% formamide; 1x Denhardt's solution; 0.25 mg/ml Baker's yeast RNA; 0.1 mg/ml Salmon sperm DNA in 5x SSC buffer) for 2 hours at room temperature in a humidified chamber. Slides were dried and hybridization buffer containing 100 ng of DIG-labeled probe were added, coverslipped and incubated at 70°C over night. Post-hybridization, slides were treated as follows: rinsed in 0.2x SSC buffer for 1 hour at 72°C, washed with 0.2x SSC buffer at room temperature for 5 minutes, washed with B1 buffer (100 mM Tris HCl pH 7.5; 150 mM NaCl) for 5 minutes, equilibrated with 10% heat-inactivated normal goat serum (HINGS) in B1 buffer for 1 hour, washed with B1 buffer three times and incubated with anti-DIG antibody (Roche) at 1/5000 in 1% HINGS in B1 buffer for 3 hours in a humidified dark chamber at room temperature. For signal detection, slides were washed with B1 buffer three times, equilibrated with B3 buffer (40 mM Tris HCl pH 9.5; 40 mM NaCl; 20 mM $MgCl_2$) for 15 minutes, dried, developing solution (0.24 mg/ml tetramisole hydrochloride; 0.35 mg/ml NBT; 0.18 mg/ml BCIP in B3 buffer) was added, coverslipped and kept in a dark chamber at room temperature until signal was detected. To stop the reaction, slides were incubated in ddH_2O for 20 minutes at room temperature four times and mounted with prewarmed Glycergel (Agilent).

Three-dimensional positional analysis

Three-dimensional positional analysis was performed as previously described (Dewitz et al., 2018). Briefly, for the embryonic analysis, lumbar levels L1 - L3 of e13.5 spinal cords were analyzed by cutting 16 μm consecutive cryosections and performing immunostaining with Isl1 antibody for LMCm neurons and Hb9 antibody for LMCl neurons. Images were acquired using a Zeiss LSM800 confocal microscope. Regions of interest corresponding to each section and consisting of 4 - 8 tiles, depending on the spinal cord size were defined and then imaged with a 10x air objective. Cartesian coordinates of neurons were obtained using the imaging software IMARIS 9.1. To account for differences in spinal cord size, orientation and shape, the datasets were rotated and normalized against a standardized spinal cord whose size was determined empirically (ML: 365 μm, DV: 340 μm). To align the datasets along the RC axis (z coordinate), the section where the first $Isl1^+$ LMCm neurons were observed was defined as z = 0. The rostro-caudal position of each neuron was obtained by keeping track of the order of the sections. The x, y and z coordinates were then used to digitally reconstruct the distribution of the neurons. The same method was applied to postnatal datasets (motor pools positional analysis and rabies tracing analysis) using 40 μm cryosections. The border between L4 and L5 (motor pools) or T1 and T2 (RV tracing) was defined as z = 0 and consecutive sections up to 2mm in the caudal (motor pools) or rostral (RV tracing) direction were analyzed, respectively. The size of the standardized spinal cord was adjusted to ML: 1000 μm, DV: 700 μm (motor pools) or ML: 1000 μm, DV: 500 μm (RV tracing).

Positional datasets were analyzed using custom scripts in "R project" (R Foundation for Statistical Computing, Vienna, Austria, 2005). In particular, contour and density plots were generated using the "ggplot2" package, which estimates the two-dimensional Gaussian density for the distribution of the given values. Correlation analysis was done with the "corrplot" package, which calculates the similarity between pairs of experiments using the Pearson correlation coefficient. Datasets were clustered hierarchically.

QUANTIFICATION AND STATISTICAL ANALYSIS

Statistical details about experiments can be found in figure legends. Unless otherwise stated, quantifications were performed by averaging parameters of three biological replicates per genotype. Significance was determined by applying unpaired, two-tailed t test. Significance was defined as: $p < 0.05$ = *; $p < 0.01$ = **; $p < 0.001$ = ***. Statistical analyses were performed with GraphPad Prism v7.2.

In order to account for differences in size and shape of the spinal cords, the extent of afadin/phalloidin expression and the length of dorsal and ventral gray matter in *afadin* $^{fl/fl}$ *Wnt1* mice were normalized against the total dorso-ventral extent of gray matter. Measurements of five sections per animal were averaged.

Cell Reports, Volume *31*

Supplemental Information

Afadin Signaling at the Spinal Neuroepithelium Regulates Central Canal Formation and Gait Selection

Sophie Skarlatou, Coralie Hérent, Elisa Toscano, César S. Mendes, Julien Bouvier, and Niccolò Zampieri

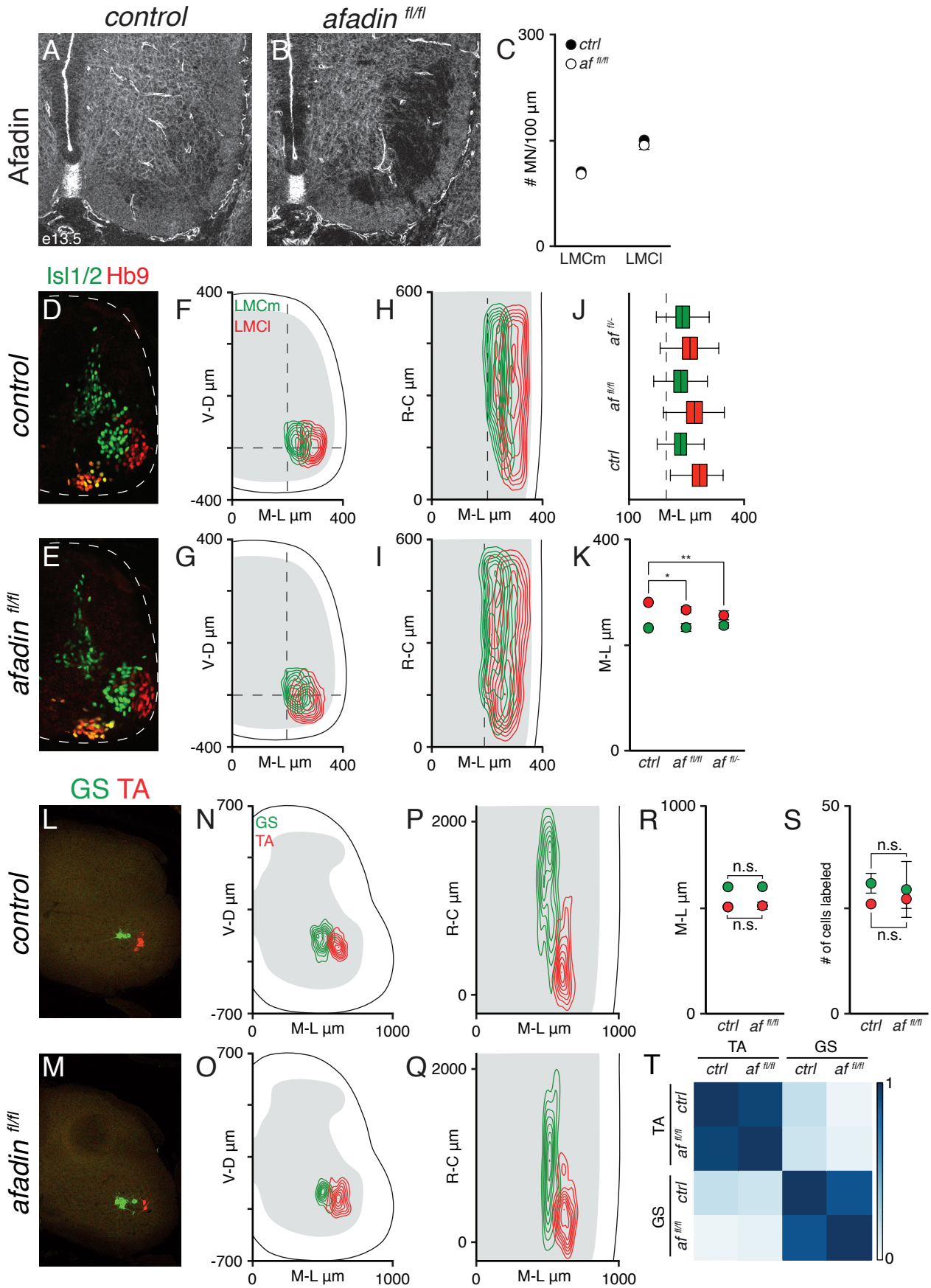
control
afadin fl/fl
Afadin
A
B
e13.5
C
ctrl
af fl/fl
MN/100 µm
300
0
LMCm
LMCl
Isl1/2 Hb9
control
afadin fl/fl
D
E
F
G
H
I
J
K
LMCm
LMCl
V-D µm
R-C µm
M-L µm
400
-400
600
100
af fl/-
ctrl
**
*
GS TA
L
M
N
O
P
Q
R
S
T
GS
TA
700
-700
1000
2000
50
n.s.
# of cells labeled

Figure S1

Figure S1. Afadin elimination does not affect motor neuron development (related to Figure 1).

A and B) Afadin expression in e13.5 control (A) and *afadin*$^{fl/fl}$ (B) spinal cords.

C) Average number of medial and lateral LMC neurons (LMCm and LMCl) per 100 µm in control and *afadin*$^{fl/fl}$ embryos (mean ± SEM; t-test, $p > 0.05$; $n = 3$ for each genotype).

D and E) Transverse sections showing Isl1^{+} LMCm and Hb9^{+} LMCl neurons in e13.5 control (D) and *afadin*$^{fl/fl}$ (E) hemicords.

F and G) Transverse contour density plots of Isl1^{+} LMCm (green) and Hb9^{+} LMCl (red) neurons in control (F) and *afadin*$^{fl/fl}$ (G) embryos.

H and I) Longitudinal contour density plots of Isl1^{+} LMCm (green) and Hb9^{+} LMCl (red) neurons in control (H) and *afadin*$^{fl/fl}$ (I) embryos.

J) Boxplots showing medio-lateral distribution of LMCm and LMCl neurons in control, *afadin*$^{fl/fl}$ and *afadin*$^{fl/-}$ (*afadin*$^{fl/-}$ dataset from Dewitz et al., 2018) embryos.

K) Average medio-lateral position of LMCm (green) and LMCl (red) neurons in control, *afadin*$^{fl/fl}$ and *afadin*$^{fl/-}$ (*afadin*$^{fl/-}$ dataset from Dewitz et al., 2018) embryos.

L and M) CTB-labeled GS (Alexa-488) and TA (Alexa-555) motor neurons in control (L) and *afadin*$^{fl/fl}$ (M) adult mice.

N and O) Transverse contour density plots of GS (green) and TA (red) motor neurons in control (N) and *afadin*$^{fl/fl}$ (O) adult mice.

P and Q) Longitudinal contour density plots of GS (green) and TA (red) motor neurons in control (P) and *afadin*$^{fl/fl}$ (Q) adult mice.

R) Average medio-lateral position of GS (green) and TA (red) motor neurons in control and *afadin*$^{fl/fl}$ adult mice (mean ± SEM; t-test, $p > 0.05$; $n = 3$).

S) Average number of GS (green) and TA (red) cells labeled in control and *afadin* $^{fl/fl}$ adult mice (mean ± SEM; t-test, $p > 0.05$; $n = 3$).

T) Correlation analysis of GS and TA neurons Cartesian coordinates in control and *afadin* $^{fl/fl}$ adult mice. Scale bar indicates correlation values.

edio-lateral axis (n = 3).

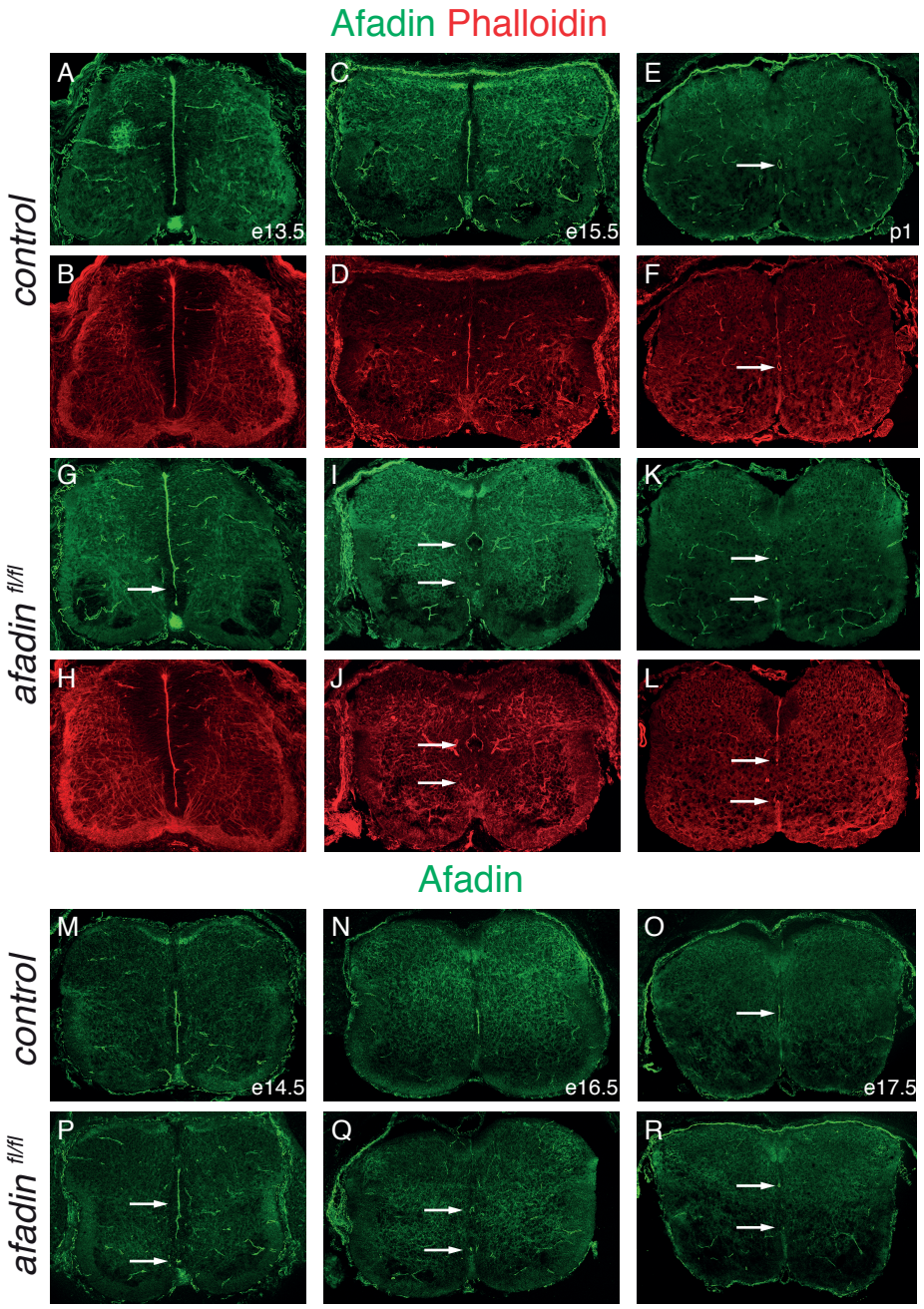
Afadin Phalloidin
control
afadin fl/fl
A
B
C
D
E
F
G
H
I
J
K
L
e13.5
e15.5
p1
Afadin
control
afadin fl/fl
M
N
O
P
Q
R
e14.5
e16.5
e17.5

Figure S2

Figure S2. Central canal development upon elimination of afadin in motor neuron progenitors (related to Figure 3).

A - F) Transverse sections of e13.5 (A, B), e15.5 (C, D) and p1 (E, F) control spinal cords showing afadin (A, C, and E) and phalloidin (B, D and F) expression.

G - L) Transverse sections of e13.5 (G, H), e15.5 (I, J) and p1 (K, L) afadin$^{fl/fl}$ spinal cords showing afadin (G, I and K) and phalloidin (H, J and L) expression.

M - O) Transverse sections of e14.5 (M), e16.5 (N) and e17.5 (O) control spinal cords showing afadin expression. Arrow points to the developing central canal.

P - R) Transverse sections of e14.5 (P), e16.5 (Q) and e17.5 (R) *afadin*$^{fl/fl}$ spinal cords showing afadin expression. Arrows point to the developing central canals.

lateral axis (n = 3).

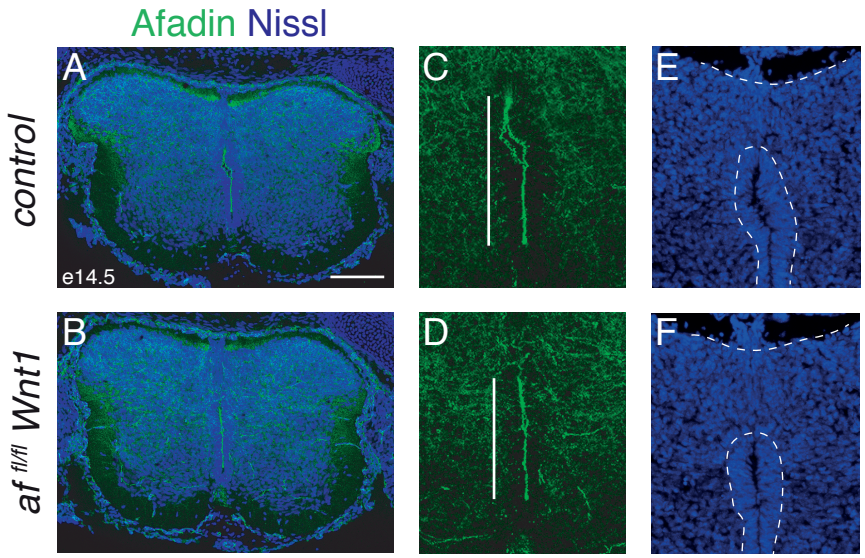

Figure S3

Figure S3. Afadin has a general role in regulating the organization of the midline (related to Figure 4).

A and B) Transverse sections of e14.5 control (A) and *af*$^{fl/fl}$ *Wnt1* (B) spinal cords. Scale bar represents 100 μm.

C and D) Afadin expression in the developing central canal area of the images in A (C) and B (D). Bars represent extent of afadin expression.

E and F) Nissl staining in the dorsal midline area of the images in A (E) and B (F). Dashed lines delineate the neuroepithelium and the border between the ventral grey and white matter.

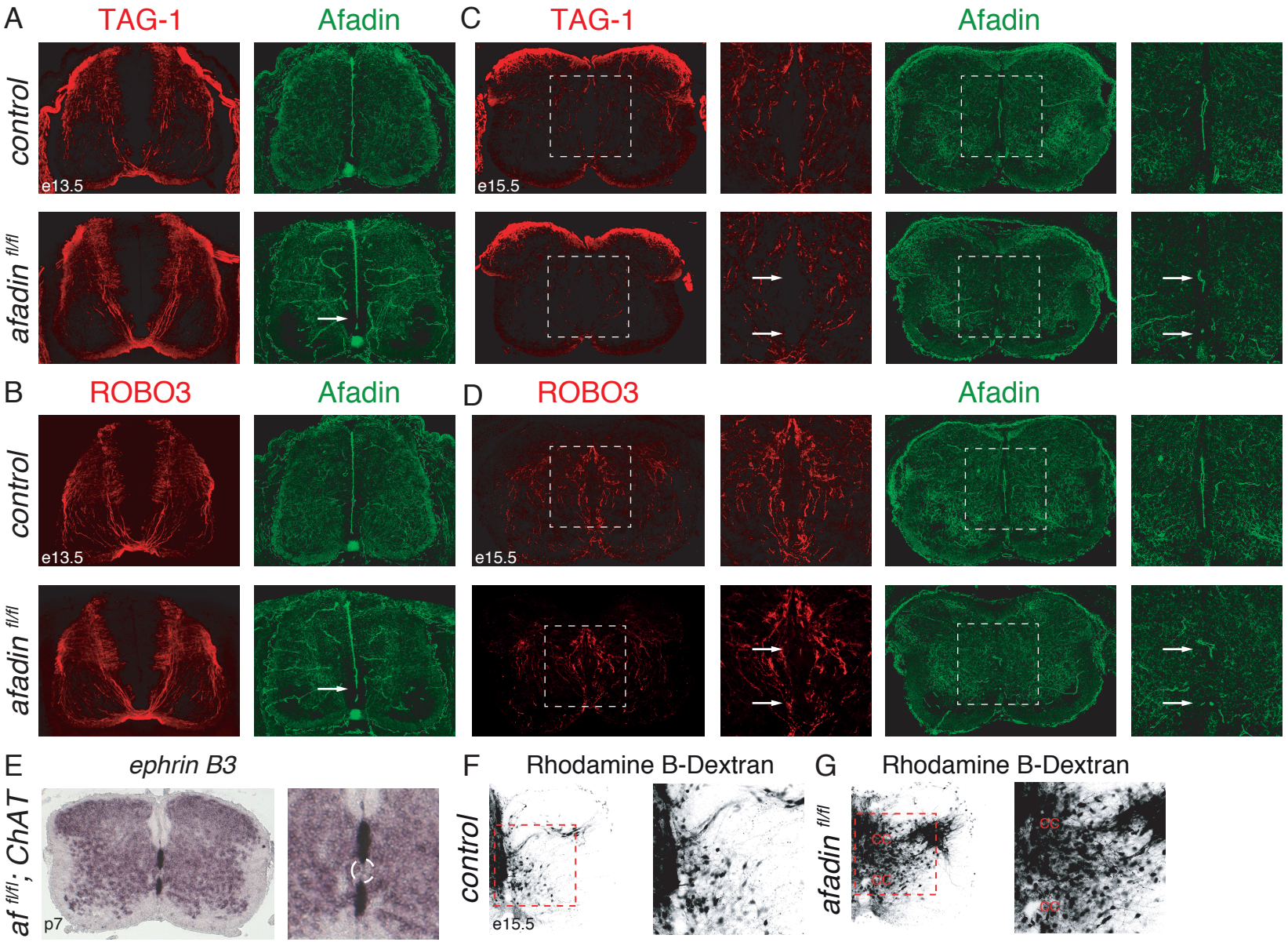
A
TAG-1
Afadin
C
TAG-1
Afadin
control
afadin fl/fl
e13.5
e15.5
B
ROBO3
Afadin
D
ROBO3
Afadin
control
afadin fl/fl
e13.5
e15.5
E
ephrin B3
af fl/fl; ChAT
p7
F
Rhodamine B-Dextran
control
e15.5
G
Rhodamine B-Dextran
afadin fl/fl
cc
cc
cc

Figure S4

Figure S4. Analysis of commissural axon organization in afadin $^{fl/fl}$ mice (related to Figure 5).

A) Transverse sections of e13.5 control and *afadin* $^{fl/fl}$ spinal cords showing TAG-1 (left) and afadin (right) expression. Arrow points to the pMN.

B) Transverse sections of e13.5 control and *afadin* $^{fl/fl}$ spinal cords showing ROBO3 (left) and afadin (right) expression. Arrow points to the pMN.

C) Transverse sections of e15.5 control and *afadin* $^{fl/fl}$ spinal cords and higher magnification of the central canal area showing TAG-1 (left) and afadin (right) expression. Arrows point to the central canals.

D) Transverse sections of e15.5 control and *afadin* $^{fl/fl}$ spinal cords and higher magnification of the central canal area showing ROBO3 (left) and afadin (right) expression. Arrows point to the central canals.

E) Left panel: Ephrin B3 mRNA expression in a p7 *af* $^{fl/fl}$ *ChAT* spinal cord. Right panel: Magnification of the central canal area. Central canal is delineated by a dashed line.

F) Transverse section of an e15.5 control hemicord (left) and higher magnification of central canal area (right) showing tracing of spinal interneurons by rhodamine dextran.

G) Transverse section of an e15.5 *afadin* $^{fl/fl}$ hemicord (left) and higher magnification of central canal area (right) showing tracing of spinal interneurons by rhodamine dextran.

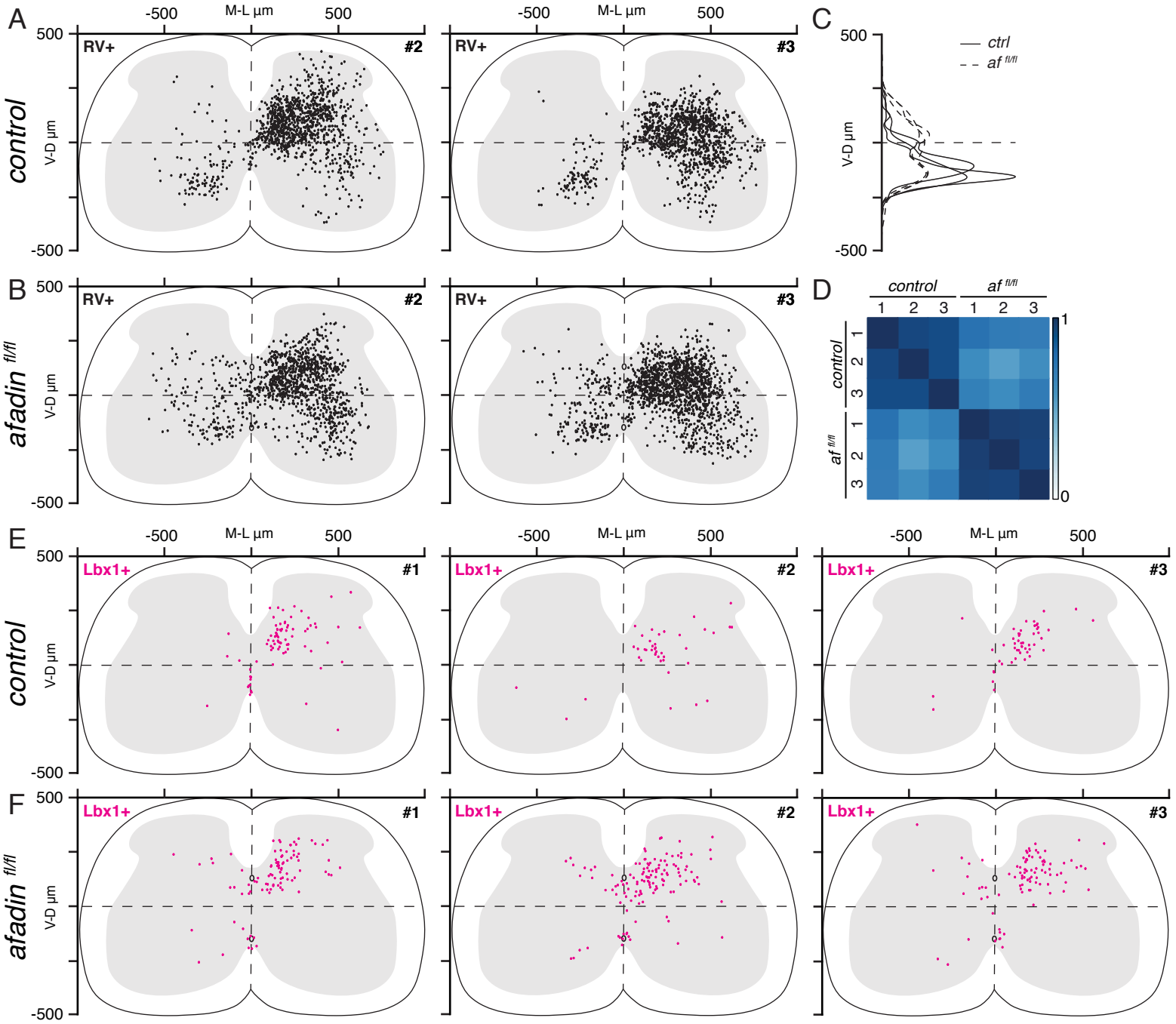
A
B
C
D
E
F
control
afadin fl/fl
RV+
Lbx1+
#1
#2
#3
M-L µm
V-D µm
-500
500
ctrl
af fl/fl
1
0

Figure S5

Figure S5. Premotor connectivity maps in control and afadin $^{fl/fl}$ mice (related to Figure 6).

A and B) Digital reconstruction of premotor interneurons positions in two control (A) and *afadin* $^{fl/fl}$ (B) mice.

C) Dorso-ventral density analysis of contralateral rabies-labeled premotor interneurons in control and *afadin* $^{fl/fl}$ mice (n = 3; each trace represents one animal).

D) Correlation analysis of rabies-labeled premotor interneuron cartesian coordinates in control and *afadin* $^{fl/fl}$ mice. The scale indicates correlation values.

E and F) Digital reconstruction of rabies^{+}/Lbx1^{+} premotor interneuron positions in three control (E) and *afadin* $^{fl/fl}$ (F) mice.

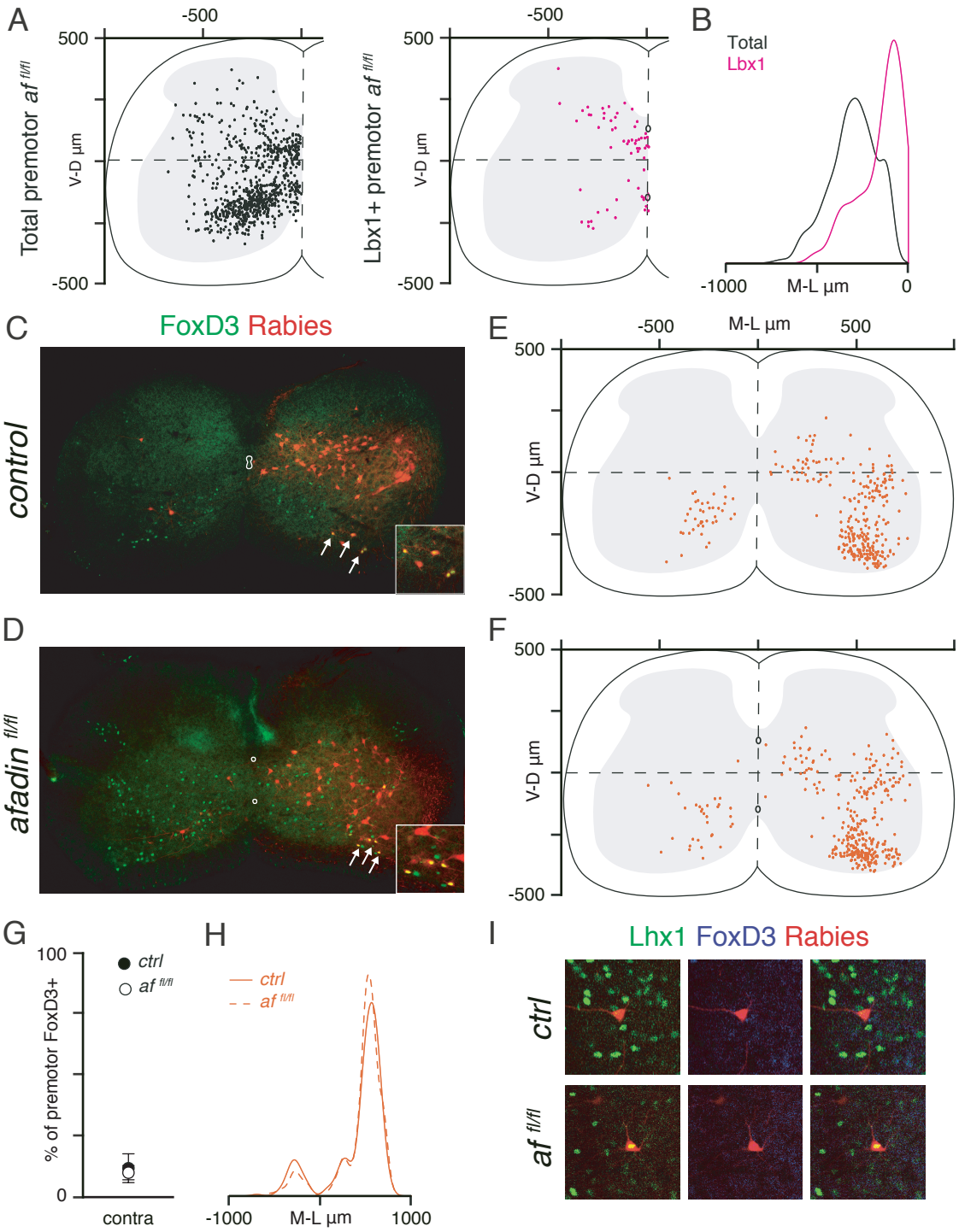
A
-500
500
V-D µm
-500
Total premotor af fl/fl
Lbx1+ premotor af fl/fl
B
Total
Lbx1
-1000
M-L µm
0
C
FoxD3 Rabies
control
D
afadin fl/fl
E
-500
M-L µm
500
F
G
100
% of premotor FoxD3+
ctrl
af fl/fl
0
contra
H
I
Lhx1 FoxD3 Rabies
ctrl
af fl/fl

Figure S6

Figure S6. FoxD3^{+} premotor interneuron connectivity is unaffected in afadin$^{fl/fl}$ mice (related to Figure 7).

A) Left panel: Digital reconstruction of total contralateral premotor interneurons mice (n = 3). Right panel: Digital reconstruction of rabies^{+}/Lbx1^{+} subset in *afadin*$^{fl/fl}$ mice (n = 3).

B) Medio-lateral density analysis in the contralateral side of total (black) and rabies^{+}/Lbx1^{+} (magenta) premotor interneurons in *afadin*$^{fl/fl}$ mice (n = 3 for each).

C and D) Ipsilateral transverse sections of a control (C) and an *afadin*$^{fl/fl}$ (D) spinal cord showing rabies-labeled premotor interneurons and FoxD3 expression. Arrows are pointing at double positive cells magnified in the insets.

E and F) Digital reconstruction of rabies^{+}/FoxD3^{+} premotor interneuron positions in control (E) and *afadin*$^{fl/fl}$ (F) mice (n = 3).

G) Percentage of contralateral rabies^{+}/FoxD3^{+} premotor interneurons (mean ± SEM; t-test, $p > 0.05$; n = 3).

H) Medio-lateral density analysis of rabies^{+}/FoxD3^{+} premotor interneurons in control and *afadin*$^{fl/fl}$ mice (n = 3).

I) Representative images of a premotor interneuron in the dorsal contralateral quadrant of a control and an *afadin*$^{fl/fl}$ spinal cord stained for Lhx1 and FoxD3.

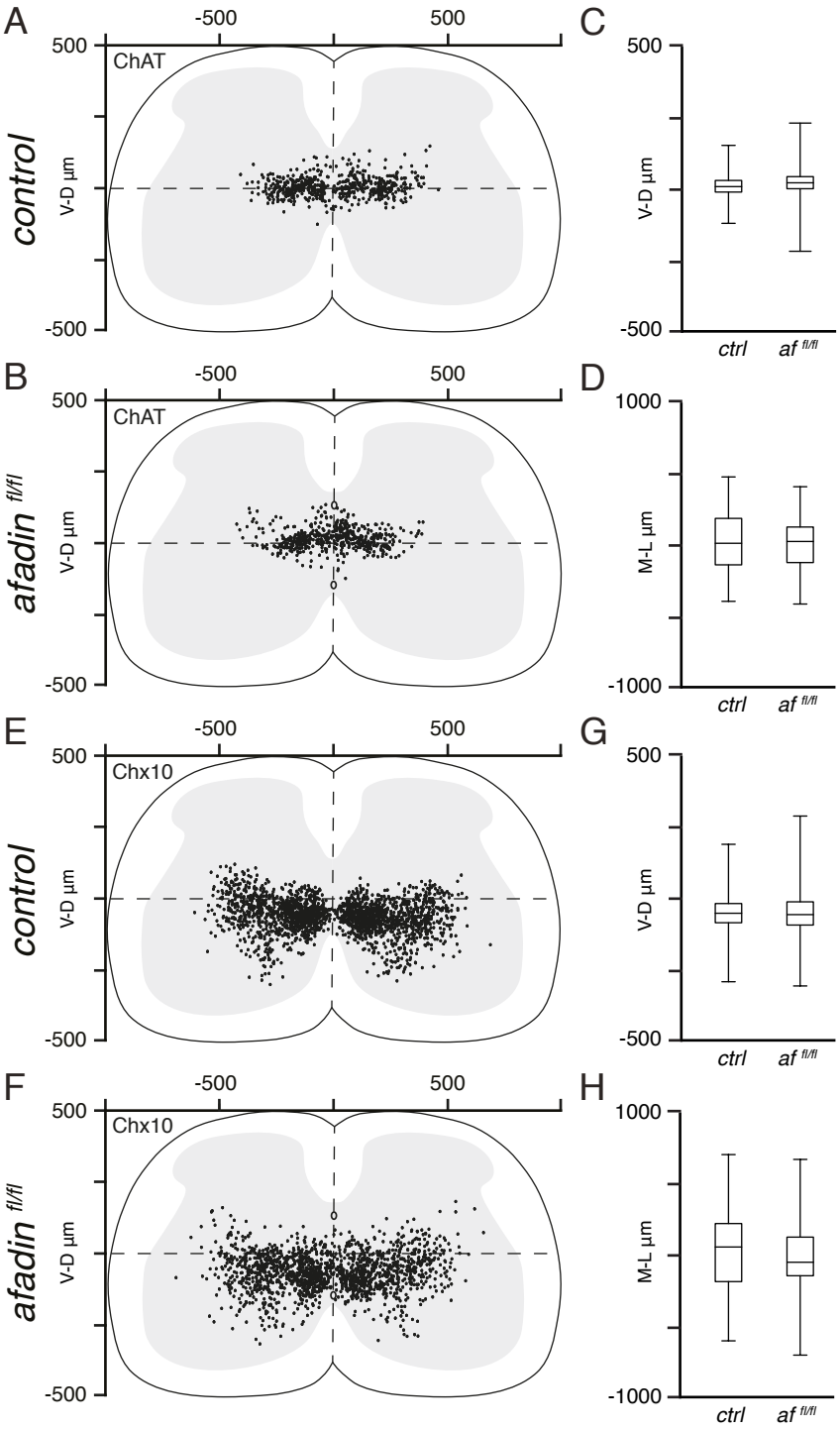
A
-500
500
500
ChAT
control
V-D µm
-500
C
500
V-D µm
-500
ctrl
af fl/fl
B
-500
500
500
ChAT
afadin fl/fl
V-D µm
-500
D
1000
M-L µm
-1000
ctrl
af fl/fl
E
-500
500
500
Chx10
control
V-D µm
-500
G
500
V-D µm
-500
ctrl
af fl/fl
F
-500
500
500
Chx10
afadin fl/fl
V-D µm
-500
H
1000
M-L µm
-1000
ctrl
af fl/fl

Figure S7

Figure S7. Positional organization of interneuron subtypes is not perturbed in afadin $^{fl/fl}$ mice (related to Figure 7).

A and B) Digital reconstruction of ChAT^{+} interneuron positions in control (A) and *afadin* $^{fl/fl}$ (B) mice (n = 3).

C) Boxplots showing distribution of ChAT^{+} interneurons in control and *afadin* $^{fl/fl}$ mice along the dorso-ventral axis (n = 3).

D) Boxplots showing distribution of ChAT^{+} interneurons in control and *afadin* $^{fl/fl}$ mice along the medio-lateral axis (n = 3).

E and F) Digital reconstruction of Chx10^{+} interneuron positions in control (E) and *afadin* $^{fl/fl}$ (F) mice (n = 3).

G) Boxplots showing distribution of Chx10^{+} interneurons in control and *afadin* $^{fl/fl}$ mice along the dorso-ventral axis (n = 3).

H) Boxplots showing distribution of Chx10^{+} interneurons in control and *afadin* $^{fl/fl}$ mice along the medio-lateral axis (n = 3).

Supplemental Table 1. Related to Figure 6 and 7.

Number of neurons labeled in each rabies experiment performed (The ChAT^{+} datasets have also been used for total premotor neuron analysis in Figures 6A-J and S5A-D).

Animal	Experiment	Total	Ipsi	Contra
Control #1	ChAT	1128	1017	111
Control #2		1179	1075	104
Control #3		968	913	55
afadin $^{fl/fl}$ #1		1101	924	177
afadin $^{fl/fl}$ #2		1585	1344	241
afadin $^{fl/fl}$ #3		1478	1269	209
Control #1	Lbx1	846	753	93
Control #2		743	704	39
Control #3		677	624	53
afadin $^{fl/fl}$ #1		1070	984	86
afadin $^{fl/fl}$ #2		1730	1566	164
afadin $^{fl/fl}$ #3		1569	1398	171
Control #1	Lhx1/FoxD3	1933	1691	242
Control #2		1175	1053	122
Control #3		667	635	32
afadin $^{fl/fl}$ #1		854	789	65
afadin $^{fl/fl}$ #2		1677	1436	241
afadin $^{fl/fl}$ #3		1875	1582	293
Control #1	Chx10	1740	1599	141
Control #2		2504	2308	196

Control #3		1160	1102	58
Control #4		1635	1464	171
afadin $^{fl/fl}$ #1		1782	1552	230
afadin $^{fl/fl}$ #2		2066	1811	255
afadin $^{fl/fl}$ #3		2190	1940	250
afadin $^{fl/fl}$ #4		1791	511	280